International Journal of Disaster Risk Reduction 138 (2026) 106110

Contents lists available at ScienceDirect

International Journal of Disaster Risk Reduction

journal homepage: www.elsevier.com/locate/ijdrr

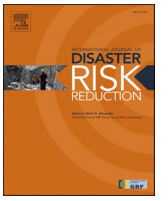

Design of a virtual test bed for the Italian territory: Proof of concept for multi-hazard scenarios effects in the context of a national resilience assessment

Isabella Serena Liso [a,1], Rita Tufano [b,1], Giovanni Poneti [c], Elena Scacchia [d], Rosa Colacicco [a,*], Valeria Lo Presti [e,**], Giuseppe Bausilio [b], Silvia Massaro [f], Francesco Neglia [a], Giovanni Scardino [a], Filippo Zaniboni [g], Mariano Di Napoli [h], Alberto Laurenti [h], Domenico Calcaterra [b], Silvia Ceramicola [c], Francesco Latino Chiocci [i], Pierfrancesco Dellino [a], Mario Parise [a], Attilio Sulli [e], Salvatore Martino [i]

[a] Department of Earth and Geoenvironmental Sciences, University of Bari Aldo Moro, Via Orabona 4, 70125, Bari, Italy
[b] Department of Earth Sciences, Environment and Resources, University of Naples Federico II, Via Vicinale Cupa Cintia, 21, 80126, Naples, Italy
[c] National Institute of Oceanography and Applied Geophysics-OGS, Borgo Grotta Gigante 42/C, Sgonico, 34010, Italy
[d] ISPRA – Italian Institute for Environmental Protection and Research, Via Vitaliano Brancati, 48, 00144, Roma, Italy
[e] Department of Earth and Marine Sciences, University of Palermo, Via Archirafi 20, 90123, Palermo, Italy
[f] Istituto Nazionale di Geofisica e Vulcanologia, Sezione di Bologna Italy, Viale Carlo Berti Pichat, 6/2, 40127, Bologna, Italy
[g] Dipartimento di Fisica e Astronomia "A. Righi", Alma Mater Studiorum - Università di Bologna, viale Berti-Pichat 6/2, 40127, Bologna, Italy
[h] WhereTech S.r.l., Via Casilina, 98, 00182, Roma, Italy
[i] Department of Earth Sciences, University of Rome "Sapienza", Piazzale Aldo Moro, 5, 00185, Roma, Italy

ARTICLE INFO

Keywords:
Geo-hazards
Virtual test bed
Impact chain
Risk mitigation

ABSTRACT

Creating quantitative tools to assess scenarios of impacts of geological processes (such as landslides, subsidence, volcanic eruptions, earthquakes), often chained in a "domino-like" effect, is an ambitious goal for quantifying risk and, consequently, supporting effective mitigation and resilience planning.

The RETURN Project, funded by the Italian National Recovery and Resilience Plan (PNRR), integrated multidisciplinary expertise to generate such scenarios and demonstrate their feasibility through a Virtual Test Bed (VTB). The need to create this virtual demonstration environment arises from the complexity of the cause-effect relationship in natural processes while enabling the evaluation of influencing factors and parameters through scalable and territorially transposable

This article is part of a special issue entitled: Virtual Testbeds for DRM and CCA published in International Journal of Disaster Risk Reduction.

* Corresponding author. Department of Earth and Geoenvrironmental Sciences, University of Bari, 70125, Bari, Italy
** Corresponding author. Department of Earth and Marine Sciences, University of Palermo, 90123, Palermo, Italy
E-mail addresses: isabella.liso@uniba.it (I.S. Liso), rita.tufano@unina.it (R. Tufano), gponeti@ogs.it (G. Poneti), elena.scacchia@isprambiente.it (E. Scacchia), rosa.colacicco@uniba.it (R. Colacicco), valeria.lopresti@unipa.it (V. Lo Presti), giuseppe.bausilio@unina.it (G. Bausilio), silvia.massaro@ingv.it (S. Massaro), francesco.neglia@uniba.it (F. Neglia), giovanni.scardino@uniba.it (G. Scardino), filippo.zaniboni@unibo.it (F. Zaniboni), mdinapoli@wheretech.it (M. Di Napoli), alaurenti@wheretech.it (A. Laurenti), domenico.calcaterra@unina.it (D. Calcaterra), sceramicola@ogs.it (S. Ceramicola), francesco.chiocci@uniroma1.it (F.L. Chiocci), pierfrancesco.dellino@uniba.it (P. Dellino), mario.parise@uniba.it (M. Parise), attilio.sulli@unipa.it (A. Sulli), salvatore.martino@uniroma1.it (S. Martino).
[1] These authors contributed equally to this work as co-first authors.

https://doi.org/10.1016/j.ijdrr.2026.106110
Received 31 October 2025; Received in revised form 18 March 2026; Accepted 20 March 2026
Available online 27 March 2026

approaches. To this end, RETURNLAND was designed as a digital space composed a complex mosaic of territorial elements extracted from the Italian surface and broadly representative of physiographic units and the geological processes active within them. RETURNLAND was used to activate tool chains capable of producing irreversible effects on the ground surface and in the submarine environment (within the near shore), which can be addressed, through impact chains, to damage infrastructure, urban areas, and communities. Among these chains, landslide-induced tsunami and consequent coastal flooding, ash-fall and ignimbrite flow propagation, subsidence and sinkholes related to sea level rising are here presented. RETURNLAND, with its virtual space, represents part of a larger Proof of Concept of the RETURN project which, among others, includes, with the same meaning as VTB, urban realities (defined as RETURNVILLEs) and human communities.

1. Introduction

Within the framework of the Italian National Recovery and Resilience Plan, funded by the European Community for the 2023-2026 period, the RETURN project (Multi-Risk sciEnce for resilienT commUnities undeR a changiNg climate) [1] focuses, among other objectives, on natural hazards related to ground instabilities [2,3], such as landslides, sinkholes, widespread subsidence, earthquake-induced phenomena (e.g. liquefaction) and volcanic activity (e.g., tephra fallout and pyroclastic density current) [4].

In particular, the project has provided the means to systematize, starting from a substantial number of case studies available in national and international literature, analytical tools for assessing the effects caused by these processes, with the aim of producing multi-hazard scenarios. These scenarios, in turn, form the basis for quantifying impact damages and consequently serve as a foundation for developing resilience strategies for communities across the national territory.

The Italian geological and geomorphological context give rise to a variety of environments where geological hazards can manifest, depending on macro-causative factors, which in the RETURN project have been categorized into three main groups: predisposing, preparatory, and triggering factors.

Predisposing factors include all geo-structural conditions inherited from the landscape during its morpho-evolution over the last hundreds of thousands of years, as well as the structural setup inheredited from geodynamic processes such as volcanic systems and orogenic structures, with specific reference to Italian territory. These factors are considered invariant over time at the scale of the evolution of natural processes which have been accounted for.

Preparatory factors include a set of time-dependent and recurrent processes, such as thermal variations from daily to seasonal cycles, fluctuations in groundwater levels related to annual hydrological cycles, as well as phenomena causing irreversible changes in the physical properties and mechanical behavior of geomaterials, such as chemical-physical alteration due to weathering. Preparatory factors are linked to complex actions driven by climate variations over medium and long periods. Therefore, scenarios modeled over different time frames can show variable spatial distributions, as meteo-climatic conditions may change over time. Preparatory factors can gradually destabilize natural systems, leading them toward a lower state of equilibrium—for example, rock masses exposed to chemical-physical weathering or thermal stresses.

Finally, triggering factors are episodic and transient events, mostly impulsive, which drive to the final manifestation of instabilities acting on a landscape, already predisposed and prepared over time; examples include seismic activity or intense rainfall causing landslide mass detachments.

The RETURN project has opted to develop chains of analytical tools that, linked in a logical-functional sequence, reproduce the effectiveness of the factors associated with the above-mentioned three macro-categories. These tools will reinstitute maps reporting the spatial distribution of ground instabilities effects allowing to differentiate them in time windows. This last solution allows taking into account climate change effects over time.

To implement these tool chains and demonstrate their effectiveness and efficiency across the diverse geological and geomorphological contexts of Italy, RETURN has chosen to create a Virtual Test Bed (VTB) [5–7]. The goal is to develop a generalizable proof of concept for the entire country that also maximizes the impact of preparatory and triggering forces, potentially acting from local to regional scales.

The approach involved mosaicking portions of Italy's territory to classify contexts and possible ground instability effects, in order to build a single digital elevation model that, as a whole, would resemble a realistic but non-actual environment, suitable for applying analytical tools to generate scenarios affected by ground instability, earthquakes, and volcanic activity.

This VTB, called RETURNLAND, is currently the first example of a virtual territory created by mosaicking real territorial portions from a single nation. As such, it can serve as a virtual laboratory to improve these tools for designing urban systems and infrastructures interconnected to withstand the impacts of such effects.

RETURNLAND can therefore be seen as a potential service pack for enhancing territorial analysis tools and, at the same time, it functions as a demonstrator of the efficiency of territorial analysis processes. It will also host virtualizations of urban digital ecosystems (hereinafter referred to as RETURNVILLEs) whose function is to become targets for the chains of effects related to geohazards that are discussed here and that are directly represented on the environmental digital ecosystem represented by RETURNLAND.

The further potential of RETURNLAND lies in its ability to be interconnected with real test beds (such as field laboratories) that, based on monitoring systems and detection of natural processes at real-world scales, can train more sophisticated analysis tools, such as those based on machine learning algorithms [8–11].

Fig. 1. The sectors highlighted with orange boxes correspond to the key areas selected for the construction of RETURNLAND. The numbers identify the different areas: 1 – portion of Po Plain, 2 – portion of central Italy, 3 – Roccamonfina, 4 – Tavoliere di Puglia and Manfredonia Gulf, 5 – portion of Metaponto plain, 6 – portion of Calabro-Tyrrhenian margin, 7 - portion of Calabro-Ionian margin, 8 – Palermo gulf. Coordinates EPSG: 4326. Base map: Google Satellite.

These algorithms, in turn, can be trained using a hybrid approach, leveraging data from instrumental recordings and outputs from numerical simulation models. From the first, the system learns with greater awareness of what has already occurred, an "eye on the past"; while from the second, it can learn with a "look to the future," allowing it to consider possible events that are not recorded but are theoretically plausible based on physical and scientific principles.

From this perspective, RETURNLAND, equipped with machine learning capabilities, can effectively become a proof of concept for a digital twin of the territory [5,12]. The capability of this digital twin lies in its ability to project future scenarios of expected effects, thus embodying the predictive capacity of analysis tools and transforming back-analysis instruments into tools that are functional for defining and designing strategies for risk mitigation and resilience enhancement.

The potential of a virtual tool, such as the RETURNLAND digital ecosystem, with respect to sensitivity analyses of parameters and their values, lies in the possibility of avoiding considering hazard-related scenarios but of being able to design parameter-dependent scenarios (possibly worst-case scenarios) without having to attribute probabilistic significance to their occurrence.

The ambition of RETURNLAND, therefore, is to be a proof of concept endowed with artificial intelligence [13,14] that makes it a digital twin capable of forecasting effects in future scenarios, specifically aimed at capturing the impact of climate change and quantifying the potential worsening of effects related to hazardous natural phenomena previously mentioned.

In this paper, Section 2 overviews the study area design and its geomorphological background in order to show the chosen

territorial contexts. Sections 3 and 4 summarize the methods and results in demonstrating the efficiency of using RETURNLAND in coastal and volcanic frameworks. Sections 5 and 6 provide discussions and conclusions on the main results and future developments.

2. Study area design and geomorphological background

Italy exhibits an exceptional variety of landforms. Within a relatively small area (approximately 302,000 km^2), well-developed features shaped by glaciers, fluvial, coastal, aeolian, weathering, and gravitational processes coexist with landforms resulting from tectonic activity and volcanism. This geomorphological diversity is set within a geologically young and seismically active territory, characterized by heterogeneous lithology and a wide range of climatic conditions.

Mountainous and hilly regions dominate over lowland areas, largely due to the presence of the Alps and the Apennines, which extend continuously across the country and exert a strong physiographic influence owing to their elevation and spatial extent [15,16]. The Alps shield the Po Plain from cold Central European air masses, while the Apennines affect the movement of humid maritime air, particularly along the Tyrrhenian coast [17]. Both mountain systems also play a key role in determining the hydrographic system, with Alpine rivers typically being longer and having greater discharge.

Po Plain in the North constitutes the largest and most significant plain in the country. The geomorphological evolution of the plain is strongly related to the fluvial pattern migration, which is controlled by climate variations, sea level changes, and tectonics and also by man-made interventions involving land reclamation and artificial embankment construction [18]. Minor plains are also found in central and southern Italy, though they cover a much smaller portion of the national territory.

Due to its dynamic geotectonic evolution, the Italian Peninsula hosts a range of volcanic systems, both extinct and active. Etna and Stromboli remain persistently active, associated with the basaltic volcanism of the southern Tyrrhenian Sea. Other volcanoes, such as Campi Flegrei, Ischia, and Vesuvius, are currently quiescent but still active, forming part of the highly explosive Campanian volcanic province. Several large volcanic complexes, such as Monte Amiata, the Latium volcanic districts, the Pontine Islands, Monte Vulture and Roccamonfina, are now extinct. The morphology of these areas still bears clear evidence of their volcanic origin, although the original landforms have been modified to varying degrees by exogenous processes. The extent of these modifications largely depends on the time elapsed since the cessation of volcanic activity, and the volcanic features are often further obscured by dense vegetation cover [19].

The coasts of Italy stretch for about 7500 km, including the islands, and constitute the majority of the country's boundaries. The surface area of the Italian seas is comparable to, and slightly larger than, that of the land masses (approximately 350.000 km^2). In most of the Italian continental margins, below the shelf edge (around 150 m depth), the seabed slope angle increases, possibly leading to widespread submarine instability processes. Except for this common configuration, the Italian seas exhibit very different morphological characteristics. The Adriatic Sea is shallow, with a wide and mostly flat continental shelf. In contrast, the Tyrrhenian Sea has narrow continental shelves, steep slopes carved by submarine canyons and deep basin plains with underwater ridges and active volcanoes (i.e. Marsili). The Ionian Sea reaches high water depths and has a complex morphology with tectonically active margins, often associated with high seismicity [20,21].

For the development of RETURNLAND, focused on simulating ground instability and volcanic scenarios, a set of representative territorial contexts was selected. This selection also incorporates a series of case studies, referred to as Learning Examples (LEs), including advanced analyses on the characterization of predisposing factors and on the spatial and temporal quantification of susceptibility. These areas represent the country's geomorphological, geological, and meteorological diversity (Fig. 1). The geographically distributed selection ensures a robust framework for applying simulation tools under varied environmental conditions and different processes.

Po Plain (box 1, Fig. 1) is a deep sedimentary basin embedded between two main Italian mountain ridges, the Alps to the North and the Apennines to the South. The geomorphological evolution of the plain is strongly related to the fluvial pattern migration, which is controlled by climate variations, sea level changes, tectonics, and also in the past, by man-made actions involving land reclamation and artificial embankment construction [18].

The central Italy area (box 2, Fig. 1) includes a significant portion of the western sector of the central Apennines and is characterized by outcropping pelagic units and carbonates of the Meso-Cenozoic platform, and flysch sediments of the Miocene Apennine foredeep [22,23]. The area develops around the Rieti intermontane basin: a Plio-Pleistocene extensional depression aligned along the axis of the Apennines chain with a subrectangular geometry shaped by the action of NS and EW normal faults [24–27] and filled by a fluvio-lacustrine sequence 0.5–2 km thick [28]. Rieti Plain is crossed by the northward flowing Velino River and by the Farfa River, a left tributary of the Tiber River.

The Roccamonfina Volcanic Complex (RVC) (box 3, Fig. 1) is located north of Mount Massico, within the Garigliano depression, in the northwestern sector of the Campania Region [29]. It is characterized by two stages of volcanic activity that are separated by volcano-tectonic caldera collapses. After the major sector collapse of the volcano, occurred at ca. 400 ka, shoshonitic rocks erupted from cinder cones and domes both within the caldera and on the external flanks of the pre-caldera Roccamonfina volcano [30].

The Tavoliere di Puglia (box 4, Fig. 1) is an extensive alluvial plain primarily composed of Pleistocene–Holocene alluvial and marine deposits. These deposits are widespread across the Apulia region and result from the interplay between eustatic sea-level fluctuations and regional uplift during the Middle to Late Pleistocene [31]. The Manfredonia Gulf represents the offshore continuation of the Tavoliere Plain and features a gently eastward-sloping seabed. This surface is interrupted by incised valleys formed during the last glacial period [32].

The area between the Cavone River (southwest) and the Bradano River (northeast) (box 5, Fig. 1), extending from the Ionian Sea in the south to the Lucanian Apennines in the northwest, was chosen due to the significant archaeological heritage found in the territory

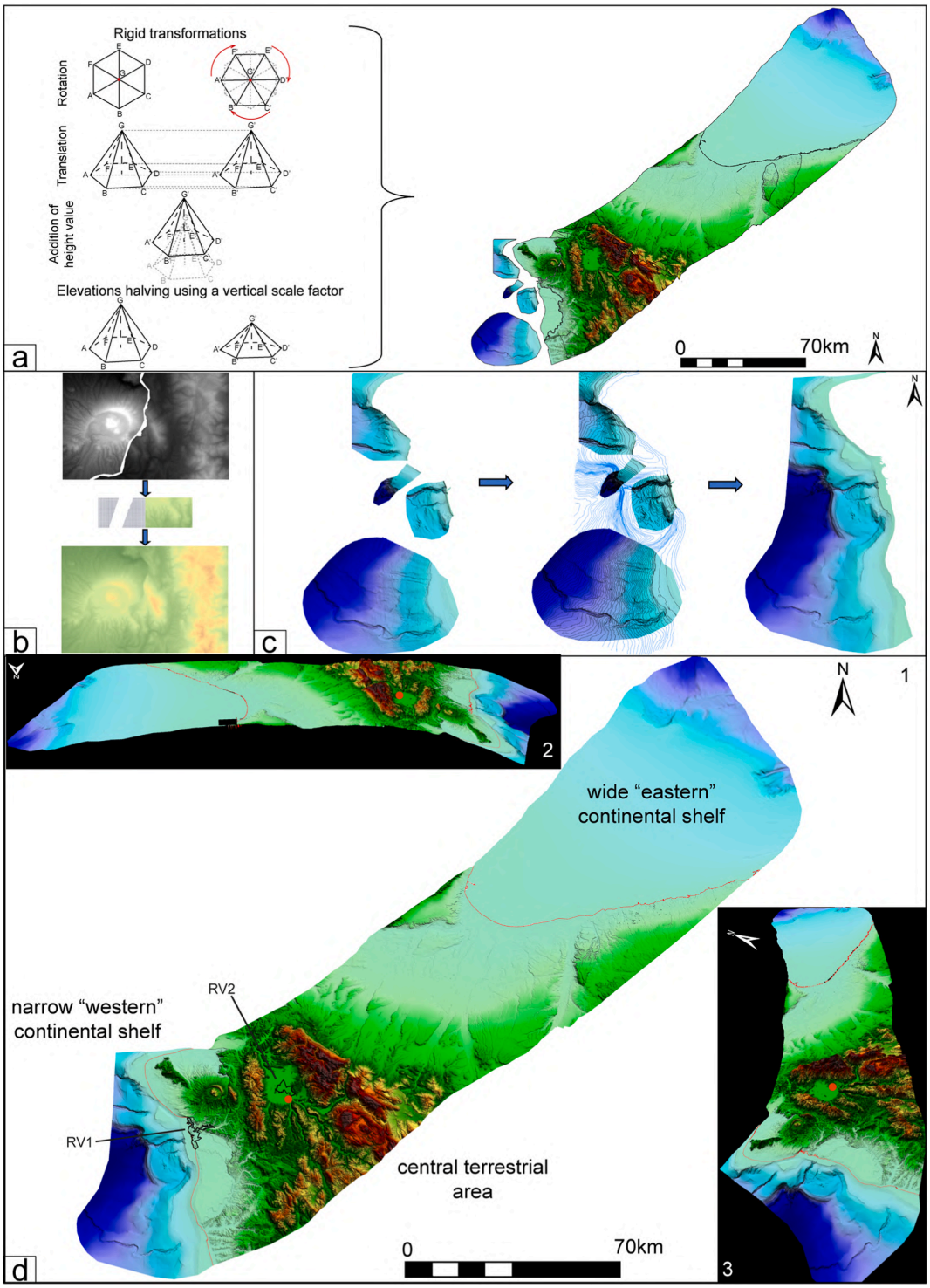

Fig. 2. a) Mosaic work of the selected DEMs. On the left, the rigid and not-rigid transformations used, on the right, view of the final patchwork. b) Example of the application of spatial interpolation techniques used for the terrestrial portion. c) Workflow applied to the "western" marine area, from left to the right: distribution of the DEMs; isobaths distribution, in black the isobaths generated automatically from the DEMS, in blue the isobaths plotted manually; the final DEM converted from the TIN. d) Final RETURNLAND; 1) 2D view; 2) 3D view from N; 3) 3D view from W.

of Metaponto. The site faces various natural hazards, including floods [33,34] and shoreline changes [35], that have endangered its cultural assets. Based on geological surveys and morpho-evolutionary analyses, the study area can be subdivided into three distinct zones, each with unique geological and geomorphological characteristics: (1) interfluvial marine terrace sequences, (2) alluvial plains of the major rivers, and (3) the coastal plain along the current shoreline [36].

The Calabro-Tyrrhenian continental margin (box 6, Fig. 1) has been shaped, since Miocene, by the activity of extensional faults [37] and is still characterized by a tectonic activity manifested through high uplift rates [38] and large and frequent earthquakes. This dynamic geological context resulted into morphologically articulate offshore areas characterized by narrow continental shelves incised by submarine canyons (i.e. Gioia-Mesima canyon system) close to the coast and steep continental slopes also characterized by the presence of structural ridges (i.e., Capo Vaticano ridge) [39].

The active Ionian margin (box 7, Fig. 1) is a tectonically active region that offers remarkable examples of submarine landslides, both on the open slope and at canyon headwalls [21,40]. This dynamic seabed is being investigated within the framework of Italian research projects MaGIc (Marine Geohazards along the Italian Coasts) [41]. Integrated seabed mapping revealed that the Ionian margin is extensively affected by numerous slide scars, indicating repeated slope failures [42]. Furthermore, several of the identified canyons appear to be connected to the onshore drainage systems [40], such as the Fiumara Corace, providing insights into the impact of climate-driven flash floods on canyon headwall retreat dynamics.

The Multibeam data acquired in the Palermo offshore (box 8, Fig. 1) produced a high-resolution DTM that enabled an accurate morpho-structural study of this marine sector [43,44]. In particular, along the continental slope, numerous morphological structures (hundreds of meters in diameter) known as submarine Pockmark have been observed. These structures are associated with fluid escape processes (water or gas) from the seafloor. Such fluid emissions are responsible for altering the geotechnical properties (cohesion, compaction, etc.) of the sediment layers they pass through, leading to the formation of incoherent sediments in correspondence with the pockmarks.

These destabilizing processes affecting the sedimentary equilibrium of the system and is responsible of the presence of several submarine landslides associated with them, showing clear retrogressive movement toward the coastal zone potentially capable of generating tsunamis.

3. Methods for RETURNLAND construction

RETURNLAND is based on a large-scale, realistic (albeit synthetic) environment. It consists of two interrelated levels exposed to the same scenarios, named RETURNVILLE and RETURNLAND. The first level consists of two virtual urban environments that incorporate features representative of Italian urban settings, one located along the coast named RV1, the other located in the mount-hilly area and named RV2 [45]. In their design, critical systems such as drainage infrastructure, electricity, road networks, and others have been considered. The RETURNVILLE level is integrated within RETURNLAND, which functions as an "environmental container" and offers a unified territorial setting reflecting both subaerial and submarine geomorphological conditions typical of the Italian territory.

RETURNLAND is a Digital Elevation Model (DEM) created by merging multiple DEMs coming from various sources and characterized by different coordinate systems.

DEMs of these areas were sourced from various regional and national databases. For central Italy and the volcanic area, DEMs were downloaded from the TINITALY website [46], available for the whole national territory at a resolution of 10 m-cell size grid (in GeoTIFF format), in the UTM WGS 84 zone 32 projection system [47–49]. A higher-resolution DEM could not be used in this area, as it was not available for at least one of the regions involved. The DEMs for the Po Plain (Emilia-Romagna, 5m resolution), part of the Puglia region (8m resolution), and the area along the Bradano River (Basilicata, 5m resolution) were obtained from the respective regional geoportals [50–52].

Bathymetric data tend to have lower resolutions compared to subaerial DTMs due to limitations related to water depth and signal penetration. Moreover, one of the main limitations of bathymetric data is the inability to acquire them too close to the coast. In fact, shallow waters hinder the navigation of survey equipment and produce sound reverberation processes that compromise signal quality.

Multibeam echosounder data from the portions of the Calabro-Tyrrhenian and Ionian margin and the Palermo gulf were acquired within the framework of the MaGIC project [41]. The Calabro-Tyrrhenian DEM includes a northern portion, comprising the Capo Vaticano ridge, and a southern one, encompassing the Gioia-Mesima canyon system. The northern portion has a resolution of 25 m while the southern one is about 15 m. DEM of the Calabro-Ionian margin, and the Palermo gulf has 15 m of resolution as well. Finally, for the Manfredonina Gulf area, the DEM was downloaded from the European Marine Observation and Data Network (EMODnet) [53], available at a resolution of 115 m.

The first step in the creation of RETURNLAND was to convert them to a single coordinate system. The WGS 84/UTM zone 33N (EPSG:32633) was chosen, being one of the most used and representative in the Italian territory. In a successive phase, the different DEMs were juxtaposed through rigid transformations, such as translations and rotations, using Global Mapper software [54]. The disposition of DEMs aimed to minimize discrepancies in the elevations to make the successive steps easier and give the final model a more homogeneous appearance (Fig. 2a). The DEMs are arranged in a “coast-to-coast” setting, typical of the geography of the Italian peninsula. From west to east the followings DEMs are included:

a) Assi submarine landslide, Gioia Tauro and Gulf of Palermo. They are arranged to form a narrow “western” continental shelf with submarine canyons close to the coastline (with a sector of the escarpment area characterized by pockmarks) and sectors of open slope;

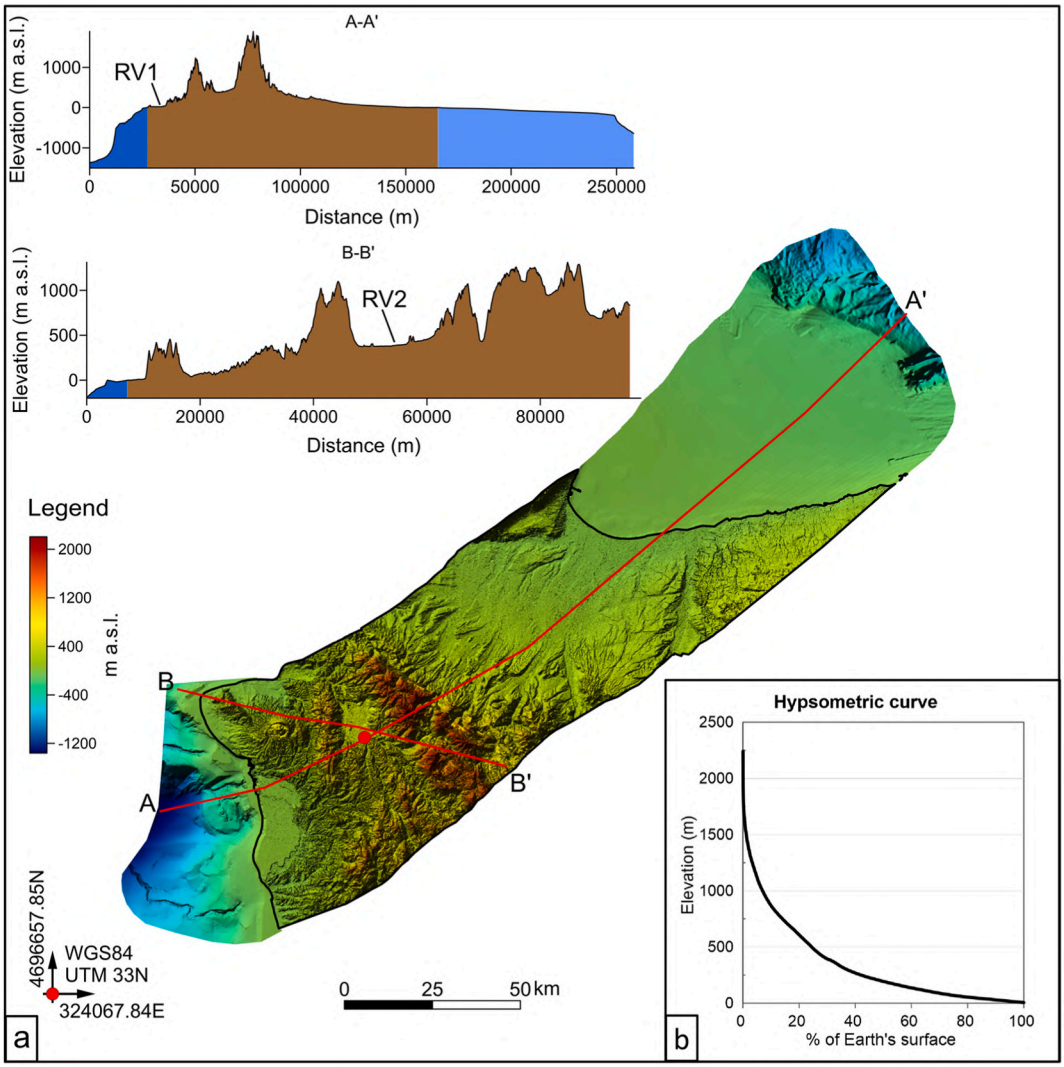

Fig. 3. a) Topographic profiles (A-A′ and B-B′) traced along the main and transversal direction of RETURNLAND; b) hypsometric curve.

b) The Emilia plain, Roccamonfina, Mountain-hill environment (Lazio), Fiumara Corace (Calabria), Apulia region, Metaponto plain (Basilicata). They are arranged to form a central terrestrial area with the highest portions in the central sections;
c) The Gulf of Manfredonia is used to form a wide "eastern" continental shelf with submarine canyons far from the coastline.

For the central terrestrial portion of RETURNLAND, further transformations consist of: 1) homogeneous increasing of the Roccamonfina DEM elevation by adding a height value to the original DEM elevation; 2) halving the elevations of the Fiumara Corace DEM using a vertical scale factor.

Following the creation of the mosaic, a sequence of geoprocessing operations was performed to address inconsistencies and fill missing data at the boundaries between adjacent DEMs.

ArcGIS Pro (Esri) [55] has been used to ensure spatial consistency and analytical reliability.

The resulting mosaicked surface was then resampled to a uniform spatial resolution of 10 m, a value chosen to balance data precision with computational efficiency. This resampling ensured that RETURNLAND represented a homogeneous topographic environment, suitable both for the current analysis and for serving as a coherent base layer in subsequent testing of related tools.

Specifically, all elevation values were converted into a feature layer of 92 million points, thus enabling the application of spatial interpolation techniques (e.g., Inverse Distance Weighting and Spline interpolation) to produce a continuous surface without gaps or voids (Fig. 2b).

Further refinement steps were carried out to remove local elevation anomalies and ensure surface smoothness. A combination of raster smoothing filters and Raster Calculator operations was employed to replace or correct specific outlier values on a zonal basis. However, the automatic tools were not always sufficient; therefore, manual editing was performed on small clusters of anomalous cells

Table 1
- Comparison between Italy [58] and RETURNLAND in terms of absolute area (km^2) and percentage distribution of the main altimetric zones (mountain, hill, plain) and the continental shelf. The final column shows the ratio between the continental shelf and land. Abbreviations: Mt = Mountain, CS = Continental Shelf.

	Absolute value (km2)						Percentage (%)			
	Land	Sea	Mt	Hill	Plain	CS	Mt	Hill	Plain	CS to land
Italy (ISTAT, 2020)	302073	350000	106276	125790	70007	88617	35	43	23	29
RETURNLAND	9309	7654	1656	4693	2960	5003	18	50	32	54

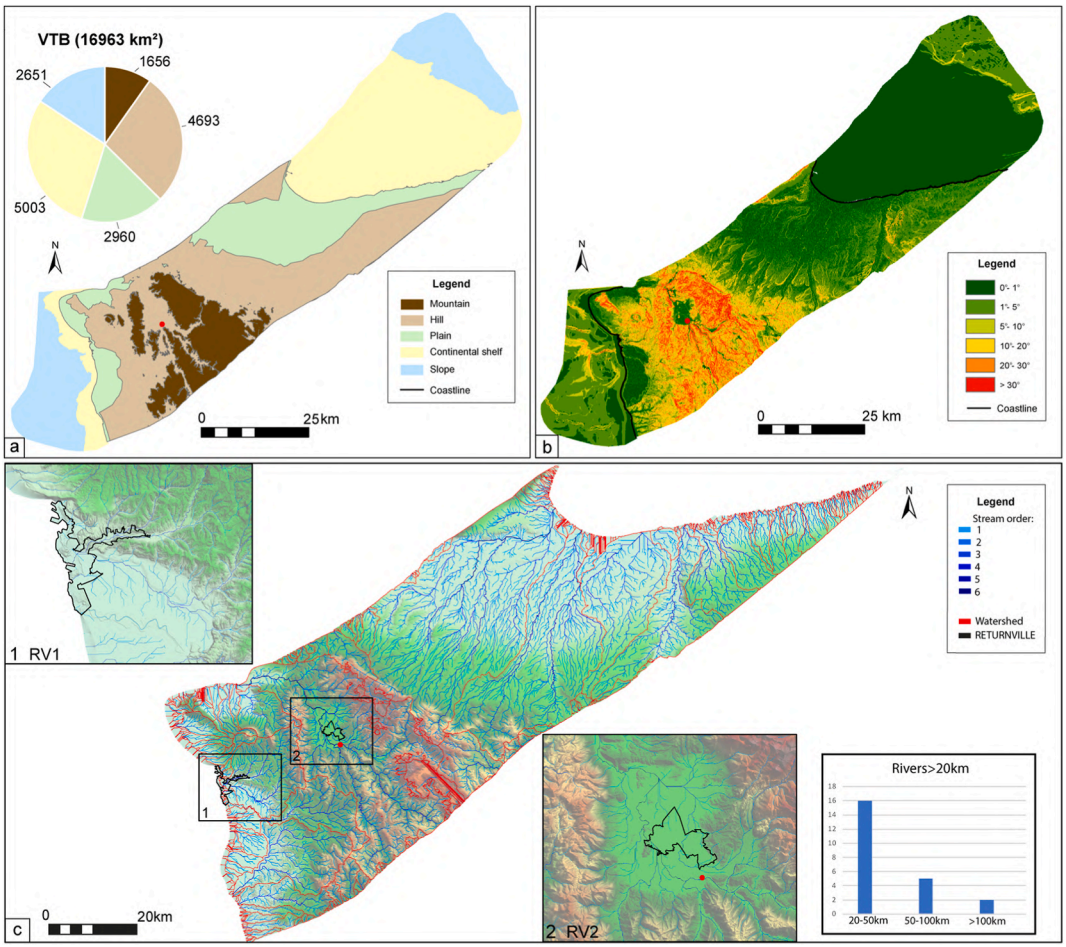

Fig. 4. a) Representation of RETURNLAND topographic areas (mountain, hill, plain, continental shelf, slope), areal extension compared to RETURNLAND total surface are reported in the pie chart; b) Slope map; c) Drainage basins dividing the RETURNLAND. 1) Detail of the hydrographic network around the RV1; 2) Detail of the hydrographic network around the RV2.

to harmonize them with the surrounding terrain values.

For the "western" marine portion of RETUNLAND, where differences in depth between the original DEMs were significant and the gaps between them wider, a different workflow was followed. In the areas where DEMs were available, isobaths were generated automatically every 20 m, while in areas where DEMs were not available the contour lines were plotted manually to ensure smoother and more realistic transitions and a better dataset continuity (Fig. 2c).

The next step was the creation of a TIN (Triangulated Irregular Network)—a vector-based model of a surface that represents the terrain through a set of irregularly distributed points (called nodes), each defined by x, y, and z coordinates. These points are connected by edges to form a network of contiguous, non-overlapping triangular facets. Together, the triangles approximate the shape of the terrain. The TIN was then converted into a DEM.

As in the case of the terrestrial part several "repair" operations were carried out on the bathymetric surface, employing both gradient-based elevation replacement tools and, where necessary, manual correction tools to ensure consistency and continuity of the

bathymetric model.

Finally, the resulting terrestrial and marine DEMs were merged using spatial interpolation techniques to produce a continuous surface. The final DEM has a cell size of 15 m and is fully available for download [56] within the Zenodo community of the project [57].

RETURNLAND spans approximately 300 km in length and 70 km in width, with elevations ranging from +2214 m to −1374 m relative to sea level (Fig. 2d).

4. Morphometric overview

To evaluate the efficiency and compare the features of RETURNLAND with the real Italian territory, some territorial analyses were conducted. First of all, two topographic profiles traced along the main and the transversal directions (Fig. 3a) allowed us to highlight the change in morphologies from sea to land, passing for the volcano, the inland plain and the main mountain belt. Moreover, the RETURNLAND hypsometry (i.e., measurement and representation of the distribution of land altitudes across the area elevation relative to sea level; Fig. 3b), shows how the land surface percentage varies from mountainous zones to coastal line. In particular, RETURNLAND presents a concave-shape curve, suggesting an eroded landscape, with a high percentage of territory that lies in lower altitudes, typically recognizable in hills and flood plains. Morphology distribution aligned with the aim of RETURNLAND to represent a typical Apennine section characterized by several coastal plains, hilly landforms and mountain peaks which rarely pass an altitude of 2000 m a.s.l.

To evaluate the representativeness of the simulated territory in relation to the Italian topographic distribution, we quantified the areal extent of mountain, hill, and plain zones, following the definitions provided in Ref. [58]. According to this classification, altimetric zones are distinguished into mountains, encompassing elevations above 600-700 m, hills with lower reliefs, and plain areas characterized by flat terrain not exceeding 300 m in altitude. The extent of the Italian continental shelves was also evaluated in comparison with that represented in the RETURNLAND, considering as continental shelf the submerged portion of the continental margin down to a depth of 150 m.

The comparison highlights some differences in the altimetric distribution between Italy and the RETURNLAND. In the latter, the hilly areas are predominant (50%), while mountainous and plain areas account for about 18% and 32%, respectively (Fig. 3b–Table 1). This indicates that the virtual model well reproduces all the altimetric zones present in the real Italian landscape, respecting the proportion between hills and plains but with a reduced representation of mountainous terrains (Table 1). The lower percentage of mountainous areas in RETURNLAND can be attributed to the fact that the model is conceived as a representation of the Italian peninsular territory, where the mountain component is primarily associated with the Apennine chain. Consequently, the omission of the representation of the Alpine domain, which is accounted for in the national statistics provided by ISTAT, leads to a proportionally lower mountain fraction in the RETURNLAND altimetric distribution.

The data also show that the ratio between the continental shelf and land is higher in RETURNLAND than in the real Italian territory. While in Italy the extent of the continental shelf corresponds to roughly 29% of the emerged areas, in the RETURNLAND this proportion rises to more than 50% (Table 1). This disproportion, however, is intentional and functional to the objectives of the virtual model, in which the analysis of marine gravitational instabilities is considered significant as the terrestrial one. Consequently, RETURNLAND was designed to ensure a greater representativeness of submarine domains, allowing for a balanced investigation of both continental and marine slope dynamics (Fig. 4a).

The slope map, divided into six slope classes, shows that the steepest gradients (20°–30°) correspond to mountainous areas, while hilly zones generally coincide with areas of 10°–20° slope, and slopes <10° are found in the plains (Fig. 4b). Regarding the marine areas, the continental shelf is characterized by slopes between 0° and 1°, reaching a maximum of 5° in the western part. In the eastern sector, slopes are generally gentler (up to 20°) compared to the western part, where gradients reach up to 30° along canyon flanks.

The RETURNLAND has a complex hydrographic system characterized by drainage basins ranging from a few km^2 to thousands of km^2 (Fig. 4c). In particular, 52 drainage basins have an area greater than 10 km^2, of which 10 are between 100 km^2 and 1000 km^2 and 3 are greater than 1000 km^2. The largest basin has an area equal to 1884 km^2. Between the rivers of RETURNLAND, 23 rivers are longer than 20 km, of which 16 are shorter than 50 km, while of the 7 rivers longer than 50 km, only 2 exceed 100 km in length. The longest is 106 km. The rivers reflect the distribution of relief. In the eastern and western parts of RETURNLAND, they tend to flow in a SW-NE direction, away from the mountainous-hilly system that dominates the central part, with mainly dendritic drainage patterns. The eastern part shows wider drainage basins and longer rivers than the western part. An exception is the drainage system in the NW area, where the conical morphology determines a mainly radial drainage pattern with relatively short rivers (generally a few kilometers long). The central part is characterized by an extensive drainage basin parallel to the direction of the mountain-hill system (NW-SE). The hydrographic network has a dendritic pattern.

The efficiency of the RETURNLAND is evaluated in coastal and volcanic areas through the application of geohazard simulation tools. The focus is on ground instability phenomena and volcanic hazards, such as tephra fallout and pyroclastic flows.

Specifically, the following paragraph illustrates the results of applying tool chains to:

1) volcanic activity-related events capable of generating a distribution of effects both in the atmosphere (ash fall) and across the relief (pyroclastic flow).
2) cascading effects capable of transferring the hazard from the original source point (in this case, located nearshore) to considerable distances inland, generating a multihazard-scenario.
3) climate-controlled scenarios of effect created, particularly, by changes in the sea level which infer to the coastal morpho-dynamics.

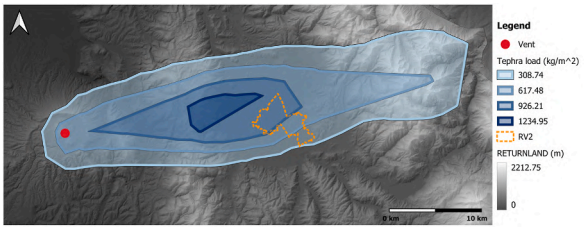

Fig. 5. Simulated tephra load (kg/m^2) generated using the FALL3D-8.0 model. The red dot marks the location of the eruptive vent, while the dotted orange perimeter indicates the RV2 zone. The background represents the topography of RETURNLAND (in meters).

5. Suitability of RETURNLAND as a PoC in volcanic and coastal environments

5.1. Volcanic simulation tools

Volcanic eruptions can generate several hazardous phenomena, such as tephra fallout and pyroclastic density currents (PDCs), which are two of the most dangerous. Although generated by different processes, both cause severe effects on infrastructure, environment, and population. Their impact change according to the eruption size and the distance from the vent. In particular, tephra load and PDC dynamic pressure can cause structural damages when they exceed the buildings resistance thresholds. For this reason, we evaluated their potential impact on RV1 and RV2 areas using advanced numerical modeling.

It should be remembered that the aim of the numerical tools application is not to replicate or reconstruct a specific eruptive event. Instead, this work aims to demonstrate the utility of the VTB as a robust framework for modeling a wide range of potential scenario.

5.1.1. Tephra fallout

To investigate the impact of tephra fallout, we considered a selected output of tephra load at ground (in kg/m^2) taken from a large number of numerical simulations carried out in Ref. [59] who assessed a long-term tephra fallout hazard assessment in southern Italy posed by the three active Neapolitan volcanoes: Somma–Vesuvius, Campi Flegrei, and Ischia. The numerical simulations were run using the Eulerian tephra dispersion model FALL3D-8.0 [60], based on the advection–diffusion–sedimentation (ADS) equations for simulating dispersion of volcanic tephra, gas, and radionuclides, with a wide range of possible model parameterization options (e.g., eruptive parameters, source model, ash aggregation, domain discretization), including the possibility to describe the gravitational spreading of the umbrella region [61].

The weather conditions were retrieved from the fifth-generation European Centre for Medium-Range Weather Forecasts global reanalysis dataset (ECMWF ERA5) [62] having a spatial resolution of $0.03^\circ \times 0.03^\circ$ and a temporal resolution of 3 h, while the volcanic scenario was randomly sampled from a set of eruptive source parameters assessed for the medium-high eruption class of Campi Flegrei as defined in literature [63,64[63,64,59].

The simulation output shown in Fig. 5 has been translated to the RETURNLAND volcanic vent (red point) showing an eruptive size compatible with the medium-high magnitude eruption class at Campi Flegrei (e.g., Agnano Monte Spina) [65] as defined in literature. The dispersal axis fully covers the RV2 with potential tephra loads in the range of 600 kg/m^2 which corresponds to a deposit thickness of ca. 60 cm (assuming a deposit density of ca. 1000 kg/m^2).

5.1.2. Pyroclastic density currents

Pyroclastic density currents are highly hazardous fast moving flows associated with medium to large magnitude explosive volcanic eruption [66]. These phenomena can originate from various eruption processes, including the collapse of eruptive columns and lava domes, directed magmatic and hydrothermal blasts, phreatic and phreatomagmatic explosions, and caldera-collapse events [67]. The solid mixtures constituting PDCs may spread around the volcano for many kilometers, severely impacting infrastructures and posing significant threats to people [68]. The main sources of hazard of PDCs arise from their high velocity, mobility, temperature and dynamic pressure [69,70], which result in partial or complete destruction of infrastructures around volcanoes and asphyxiation due to the abundance of fine, hot ash [71,72[71,72,69,67]. Understanding the mechanism governing the generation and propagation of PDCs and their interaction with buildings is fundamental for accurate risk assessment. Assessing the impact of PDCs on buildings with known resistance thresholds for walls, doors and windows can help to mitigate their effect [73]. For these reasons, the second application of RETURNLAND in a volcanic context was focused on PDCs generated by the collapse of an eruptive column on real topography, including a dock area located about 11 km from the vent (RV1). This distance mimics the real distance of the historical city of Pompeii, which was invested by PDCs during the eruption of Mount Vesuvius in Southern Italy. Model calculation was carried out using the ANSYS Fluent simulation tool [74].

Fluent is a widely used multiphase Computational Fluid Dynamics (CFD) software, which treats multiphase flows simulations with different approaches (e.g., Discrete Element Method and Two-Fluid Model). The Two-Fluid Model (TFM) was applied to the selected scenario, since it is more suitable for flows involving large numbers of particles, such as PDCs [75]. In the last decades, several authors have successfully applied TFM to volcanic phenomena [76,77[76,77,70,78,79,80–83]. TFM treats the gas and solid phase as interpenetrating continua whose motion is regulated by the Navier-Stokes Equation, which are solved for each phase (gaseous, liquid or solid) with constitutive equations accounting for the momentum and energy transfer between phases.

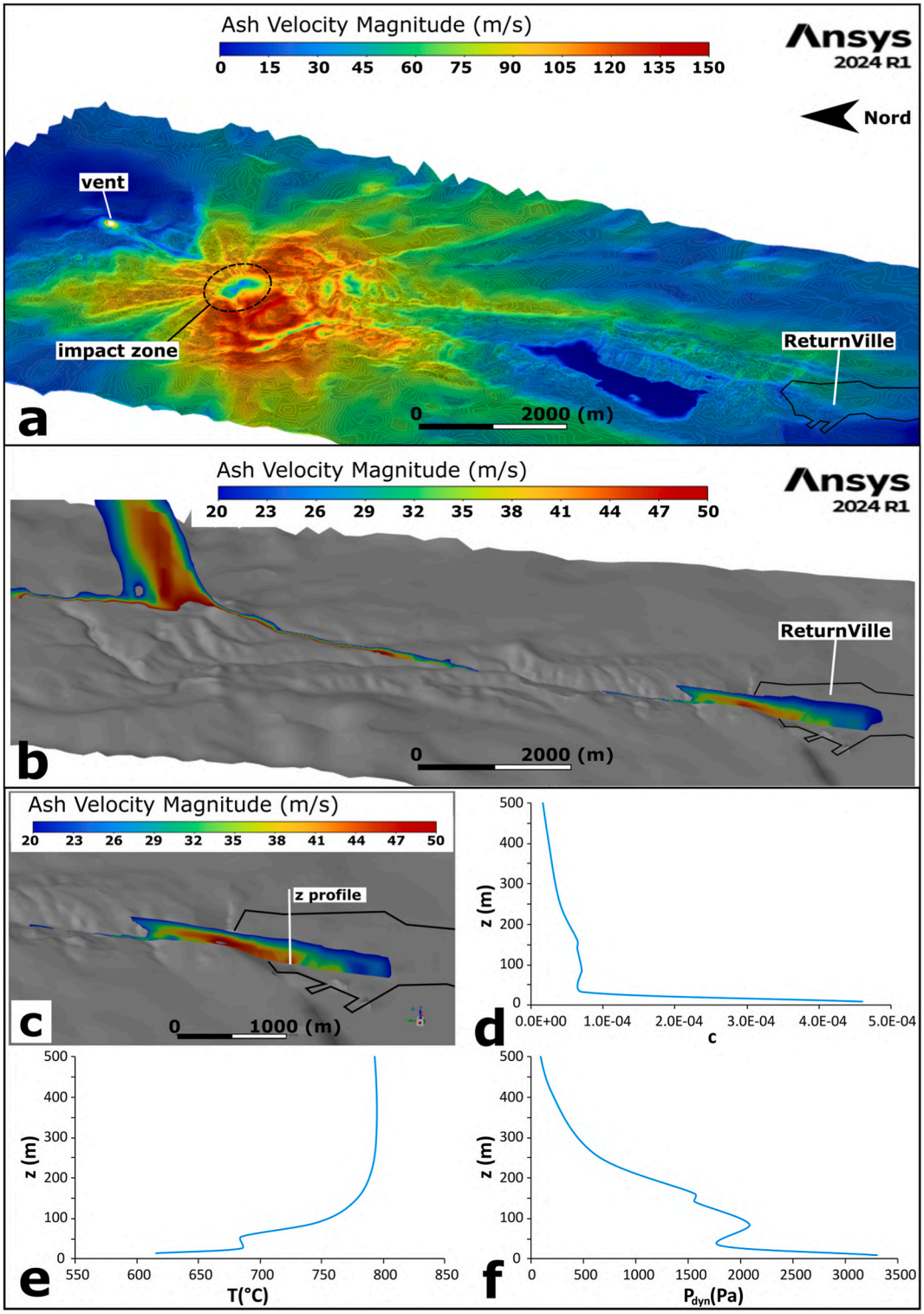

Fig. 6. a) Contour map of ash velocity magnitude at ground level, b) ash velocity magnitude along a vertical *yz*-slice, c) zoomed view of ash velocity contour in the RV1 area, vertical profile of (d) ash concentration, (e) temperature, and (f) dynamic pressure in the inundated area.

Table 2
Values for the coefficients appearing in Eq. (1), respectively for open slope and canyon head environment. The second part of the table reports the morphological characteristics of the landslide scenarios in the two considered environments (V, volume; D, initial depth; θ, initial slope).

	Open Slope	Canyon Head
ε_V	1.0	0.9
ε_D	−1.2	−0.5
ε_d	−0.5	−1.2
ε_θ	1.1	0.5
A	0.01096	0.10543
B	−0.01328	0.00280
Landslides morphology		
V (10^6 m^3)	94.3	0.84
D (m)	120	20
θ (°)	3	15

The rectangular computational domain measuring 20 km × 6 km x 7 km in the x (flow direction), y and z dimensions, respectively, consists of a body-fitted, unstructured hexcore mesh of about 1000000 cells. Local refinements were applied to the vent, collapsing region, along the main flow path, and around the dock area 11 km from the vent. Cells size in refined zones is set to 50 m, with finer cells of 10 m in the dock area, in order to capture dynamic pressures and flow behavior in detail. The flow inlet corresponds to the volcano summit within the caldera (Fig. 6a). The mass eruption rate (MER) of the inlet is set to 1.6×10^8 kg/s, which falls in the range (10^7 – 10^9 kg/s) required to generate PDCs [84]. The solid phase at the inlet has a density of 1550 kg m^{-3}, a diameter of 25 μm, and a temperature of 800 °C.

Fig. 6 shows the velocity magnitude of PDCs generated by column collapse on the reconstructed topography, with the vertical profile of dynamic pressure in the dock area. Generally, PDCs spread radially from the impact zone (dashed line, Fig. 6a) toward the domain boundaries, along the main ravines. The impact zone is recognizable by a central area of low velocities, which denotes the granular compaction phase. In this stage, the gas pressure increases, forcing lateral expansion of the mixture. The maximum simulated velocities of about 150 m s^{-1} are reached in the downstream zone adjacent to the impact area, where PDCs bypass the morphological highs before being channelized in the main ravines, reaching velocities of 70 – 100 m/s. Near the RV1 dock area (highlighted in Fig. 6a), the velocities drop to 40 – 50 m/s. Fig. 6b shows a yz-plane slice of ash velocity magnitude, including a portion of the flow impacting RV1. In this area, the flow has a thickness of about 200 m, with maximum velocities of 52 m/s. A second pulse can be seen following the main flow inundating the dock area. The presence of multiple pulses has been observed during large- and small-scale laboratory experiments [85,86]. and hypothesized for both volcaniclastic and pyroclastic deposits based on field evidence [87–89]. The arrival of different PDCs in the inundated areas concurs to the final hazard. Fig. 6c reports a zoom of the dock area, showing the flow passage over the concave-downward slope near RV1. This passage is characterized by a hydraulic jump of the flow, which decreases its velocity and increases its thickness (from supercritical to subcritical flow). Fig. 6d–f shows the vertical profile of dynamic pressures (P_{dyn}), temperatures (T) and concentrations (c) in the same area. Despite the 11 km of travelled distance from the vent to RV1, over complex terrain, the PDC retains dynamic pressures of 3.3 kPa at 10 m above the ground, with solid concentration of 5×10^{-4} and temperature of 600 °C. These values are consistent with previous studies [90,69,72] and suggest potential damage to building openings, causing the ingress of hot ashes into structures. This increases the amount of damage and poses serious risks to human health. In this case, the mechanical effects of the currents on buildings are secondary to impact of high temperatures (>500 °C) and ash concentrations, which are exacerbated by the prolonged exposure time (several minutes) during the flow passage. Furthermore, these dynamic pressures can flatten up to 90% of trees [91], making the area impassable to vehicles and severely hindering emergency services.

5.2. Landslide-tsunamis simulation in the western coastal area

The impact of landslide-generated tsunamis on coastal zones is evaluated using two specialized tools, each addressing a distinct phase of the hazard process and applied sequentially.

The LANDSLIDE-TSUNAMI tool estimates the maximum tsunami amplitude on the coastline (η) based on the morphologic characteristics of the landslide source, following the empirical expression:

$$\eta = A(V^{\varepsilon_V} \cdot D^{\varepsilon_D} \cdot d^{\varepsilon_d} \cdot \sin\theta^{\varepsilon_\theta}) + B \tag{1}$$

Where: V is the volume of the landslide; D the initial depth; θ the initial slope; d the distance from the coast. The combination of these quantities is regulated by the exponents ε_V, ε_D, ε_d and ε_θ, which account for the influence of each quantity on the tsunami genesis, as shown in Table 2.

Exponent and coefficients A and B change based on the landslide environment (open slope, OS, or canyon head, CH) (see Table 2). These values were derived by searching for the best fit between the computed values of η from Eq. (1) to reference results obtained through numerical simulations of various landslide-tsunami scenarios (see Ref. [92] for some examples of such simulations). The numerical codes are part of a well-established computational framework that has been extensively validated in previous studies

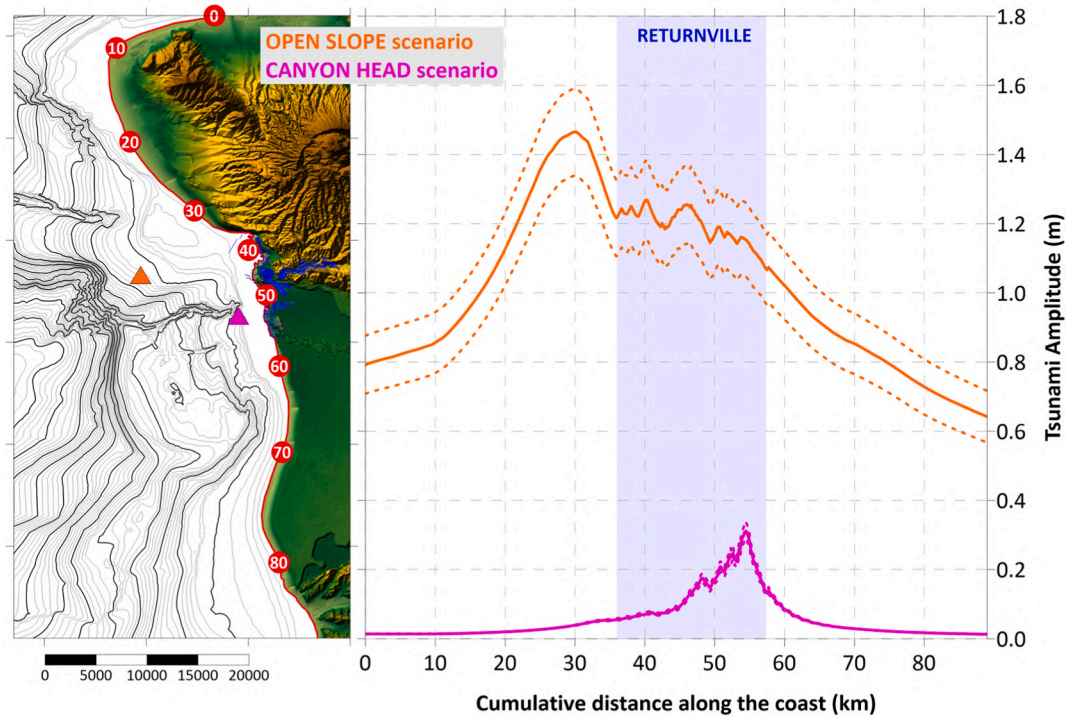

Fig. 7. Left panel) map of the coastal area of RETURNLAND with localization of the two landslide scenarios (orange triangle for open slope; magenta triangle for canyon head). The red line marks the coast, whit white labels in red circles reporting the cumulative distance along the shoreline. The blue boundaries represent the RV1 cadastral cells, used to evaluate the impact of the tsunami. Right panel) Tsunami amplitude vs cumulative distance along the coast for the open slope and canyon head environment (in orange and magenta, respectively). The blue-shaded area marks the position of RV1 along the coast. Dashed lines mark the uncertainties associated with the tool output.

[93–96] and references therein. The landslide volumes were determined based on a statistical analysis conducted along the Tyrrhenian Calabrian continental margin [97], from which Sector 6 of RETURNLAND was extracted. From the analysis and comparison of geomorphological features (i.e., scars and deposits of submarine landslides), it was found that landslides occurring at canyon heads can mobilize up to 10,10^6 m^3, whereas those on open slopes can mobilize up to 1000 10^6 m^3 [97]. We decided not to consider the maximum volume, which represents rare events, but rather volumes one order of magnitude smaller, which are statistically more abundant and therefore more representative of the landslide dynamics in the area.

The TSUNAMI FLOODING tool reconstructs the tsunami-induced flooding along 2D topographic transects extending inland from the shoreline. It is based on the Energy Method, described in Ref. [98], which considers flow energy dissipation during the inundation process. Apart from the profile describing the morphology of the coastal area, the tool needs in input the flow amplitude at the origin of the transect (which is the coastline point), and the value of the Manning's coefficient, representing resistance due to natural and anthropogenic surface roughness. A recursive procedure, starting from the computation of the maximum possible runup with the prescribed amplitude at the coast, allows us to estimate the flow depth and velocity for each point along the transect. These outputs are critical for evaluating the impact on buildings and infrastructure and are essential components of comprehensive coastal risk assessments.

5.2.1. Application of the LANDSLIDE-TSUNAMI tool

The tsunami amplitude on the coast has been assessed for two scenarios, one for each environment, which position is denoted respectively by the orange and magenta triangles in Fig. 7 (left panel). The morphological parameters introduced in Eq. (1) to obtain η are reported in Table 2, except for the distance from the source, d, which changes for each coastal point and that is computed accordingly.

The results of the tool application are displayed in the right panel of Fig. 7. As expected, the OS scenario generates significantly higher waves, consistent with the two orders of magnitude difference in volume. The highest effects occur north of RV1, at about 30 km cumulative distance along the coast, where wave amplitude reaches approximately 1.5 m. The coastal area facing the town experiences tsunami amplitudes of around 1.2 m – levels that are not catastrophic but still capable of generating strong harbor currents, potentially damaging boats and triggering local resonances that could in turn amplify the waves.

Notably, the tsunami impact is widespread across the entire analyzed coastal stretch, extending over 80 km, with wave amplitudes exceeding 80 cm. In contrast, the CH scenario produces much more localized waves, which maximum is around 30 cm in the southern part of the RV1 shoreline. In this case, the tsunami effects are largely confined to the urban costal area and negligible beyond it.

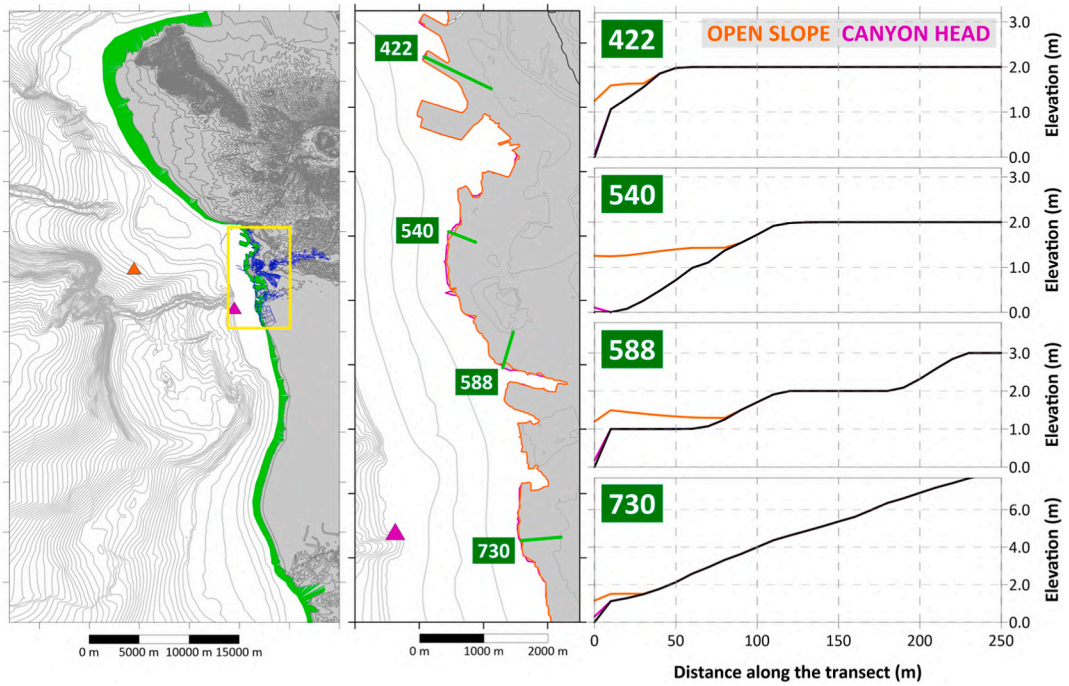

Fig. 8. Left panel) map of the coastal area of RETURNLAND with the two landslide scenarios (orange triangle - OS; magenta triangle - CH). In green the transects along which flooding is computed. The blue boundaries represent the RV1 cadastral cells. The yellow rectangle evidences the zoomed area. Central panel) Zoom on the RV1 area. The green lines mark the four transects (with the corresponding numbers) for which inundation is shown. The orange and magenta polylines represent the maximum inundation for OS and CH scenarios respectively, obtained connecting the point of maximum inundation for each transect. Right panel) Topographic profile (in black) and flooding for OS (in orange) and CH (in magenta) scenarios for the four selected transects.

5.2.2. *Application of the tsunami flooding tool*

The second step of the tsunami hazard assessment for RETURNLAND involves the application of the flooding simulation tool. Water inundation is evaluated along with 2D topographic profiles. Specifically, a set of 1170 transects has been generated (in green, Fig. 8, left panel), spaced 100 m along the shoreline and oriented approximately perpendicular to the coast, with a longitudinal resolution of 10 m. For each transect, the output from the previous tool provides the wave amplitude at the origin point, placed on the shoreline. Manning's coefficient is set to 0.030 [99], corresponding to barren land. It should be noted that the results here presented do not account for the presence of buildings or anthropogenic infrastructure, which are then neglected in this phase of the analysis.

Flooding along four representative transects, located along the RV1 coastline, is shown in Fig. 8 (central panel for their location, right panel for topographic profile). As expected, the inundation distance and runup vary depending on the local morphology. In general, the OS scenario results in more extensive inundation, with water penetrating for almost 80 m inland in certain areas (e.g., transect #540 and #588).

Moreover, the flow depth along transect#540 exceeds 1.5 m for several meters inland, indicating a potentially significant impact on population located near the shore, especially when combining this factor with flow velocity (which is not shown here). The CH scenario produces more limited flooding, consistent with the lower tsunami amplitudes observed in this case.

5.3. *Climate driven sinkholes susceptibility assessment*

The RETURNLAND virtual environment provides an integrated framework for analyzing coastal evolution and shoreline dynamics through time. By combining geological, geomorphological, and hydrodynamic data, it supports both reconstruction of past coastal changes and prediction of future trends. Two modeling applications were developed, to reconstruct past shoreline positions for assessing retreat and progradation rates, and to predict shoreline evolution up to 2175, indicating coastal flooding and landward migration due to sea-level rise. Additionally, machine learning models were applied to evaluate the influence of coastal processes on sinkhole development [100] producing predictive susceptibility scenarios linked to sea-level variations. Simulations focused on the eastern sector of RETURNLAND, a low-gradient coastal plain ideal for assessing shoreline migration and sinkhole susceptibility under rising sea-level conditions, enabling a robust evaluation of long-term stability of coastal systems.

5.3.1. *Coastal dynamics modeling: Reconstruction and projection of shoreline evolution under climate changes*

The first simulation aimed to identify a period in the past during which, within a geologically short time span, multiple phases of

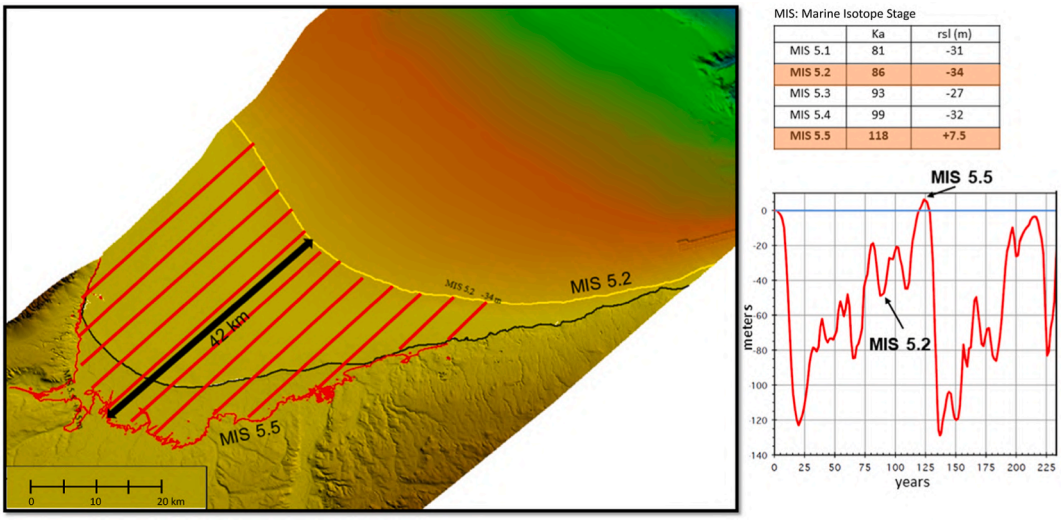

Fig. 9. The area highlighted by red lines corresponds to the territory that reached the minimum and maximum sea level during MIS 5, MIS 5.2 and MIS 5.5 respectively and that record several times the sea passage (rising and falling phases) over it.

Table 3
Column A: MIS age; column B: MIS relative sea level (Rsl) depth; column C: actual depth of MIS deposits; column D: linear distance between singular MIS peak (km).

	A	B	C	D
	(Ka)	Past Rsl depth (m)	Actual rsl (m) depth, corrected by tectonics (−0.18 mm/y)	Linear distance on map between MIS5 peak (km)
MIS 5.1	81	−31	−45	
MIS 5.2	86	−34	−49,48	≈2 landward from MIS5.2 to MIS5.1
MIS 5.3	93	−27	−43,7	≈5,2 seaward from MIS5.3 to MIS5.2
MIS 5.4	99	−32	−49,8	≈1.5 landward from MIS5.4 to MIS5.3
MIS 5.5	118	+7.5	−22	≈41 seaward from MIS5.5 to MIS5.4

sea-level rise and fall occurred. This period was identified as the Marine Isotope Stage 5 (MIS 5), between approximately 125 ka and 80 ka years ago (Fig. 9). During this relatively short interval, about 45 ka, five sea-level oscillations occurred: three transgressive and two regressive phases. The peak corresponding to MIS 5.5 is the only one among the three warm peaks during which sea level rose above the present-day level. The last Interglacial transgression in Italy occurred around 118 ka. Its imprint is still visible and recognizable in numerous geomorphological and biological markers found along the coasts, providing a unique reference for studying the vertical movements of the Italian shorelines.

The reconstruction of the paleoshorelines therefore identifies five past shorelines, whose elevations relative to the present sea level are reported in Table 3, columns A and B [101–103]. The same table also shows the current depths of the deposits associated with the five MIS 5 peaks, corrected for vertical tectonic movement at a rate of −0.18 mm/year, as shown in column C. Column D describes the linear distances measured as a function of the repeated marine regressions and transgressions from MIS 5.5 to MIS 5.1. Considering the maximum linear shoreline shift, between MIS 5.2 (sea-level minimum depth: 34 m) and MIS 5.5 (sea-level maximum depth: +7.5 m), the area affected by these numerous sea-level variations corresponds to a strip approximately 42 km wide, straddling the present-day coastline of RETURNLAND.

The second simulation performed in the RETURNLAND focused on the assessment of coastal flooding induced by future Sea-Level Rise (SLR). Flooding extents were evaluated using a bathtub model that integrates both projected SLR and Vertical Land Motion (VLM). VLM rates for the study area were obtained from InSAR and GNSS datasets from September 2014 to January 2021 and were used (i) to correct the Digital Elevation Model (DEM) of the RETURNLAND, and (ii) to estimate future vertical displacements for the years 2050, 2100, 2150, and 2175, under the assumption of a linear trend. The areas experiencing the highest subsidence display VLM rates of -7.2 mm yr^{-1}.

Sea-level rise projections were derived from CMIP6 climate models for multiple temporal horizons (2050, 2100, 2150) under two shared socio-economic pathways (SSP1–2.6 and SSP5–8.5). These trends were linearly extrapolated to 2175 (Fig. 10). The future shoreline position was then determined by applying the bathtub model to the VLM-corrected DEM, using the median SLR values from the SSP5–8.5 scenario, representing the worst-case flooding condition (Fig. 10a and b).

Model projections indicate progressive coastal inundation across the RETURNLAND area, with flooded extents of 50.5 km^2 (2050), 118.7 km^2 (2100), 147.7 km^2 (2150), and 152.3 km^2 (2175), respectively (Table 4). The most vulnerable sectors correspond to low-lying areas adjacent to the current shoreline, which are expected to undergo complete and permanent inundation, resulting in the loss

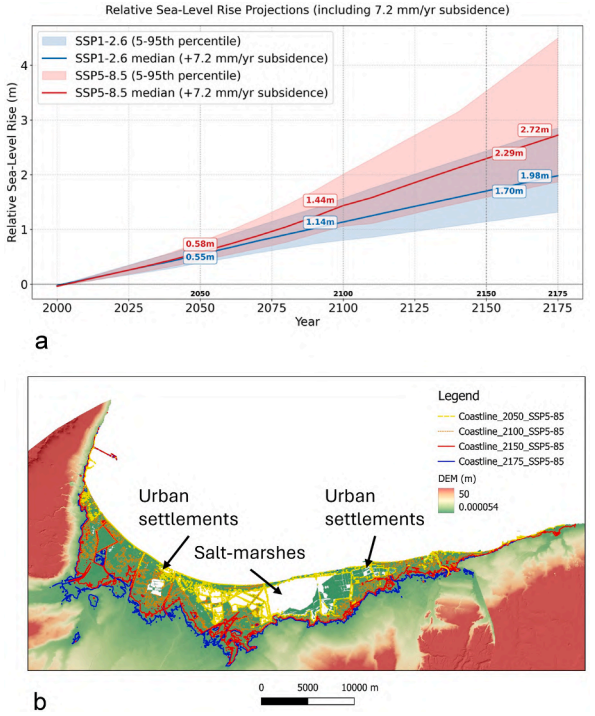

Fig. 10. a) SLR projection of CMIP6 under two different scenarios: SSP1-2.6 (blue) and SSP5-8.5 (red); b) future coastlines position, considering the SLR median values of SSP5-8.5 scenario.

Table 4
Effects of SLR and VLM across multiple future time horizons. Reported parameters include the projected shoreline displacement, VLM, the total SLR–VLM joint action, and the corresponding extension of flooded area.

Year	Projected SLR – SSP5-8.5 (m)	Ground deformation due to VLM (m)	SLR corrected with VLM (m)	Flooding surfaces (km^2)
2050	0.22	0.36	0.58	50.5
2100	0.72	0.9	1.44	118.7
2150	1.21	1.08	2.29	147.7
2175	1.46	1.26	2.72	152.3

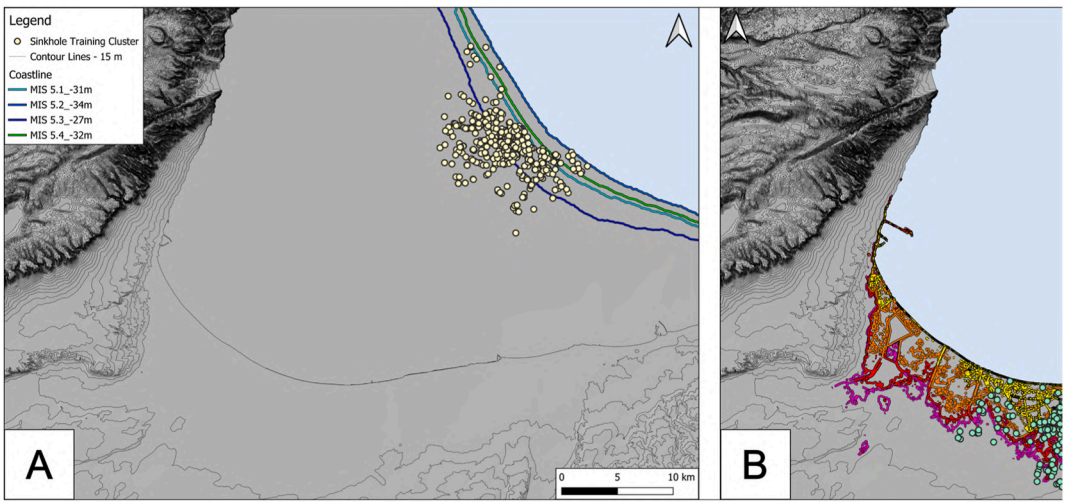

Fig. 11. Shoreline displacements and sinkholes cluster. A: training phase (MIS 5); B: predictive phase (2100, 2125, 2150 and 2175).

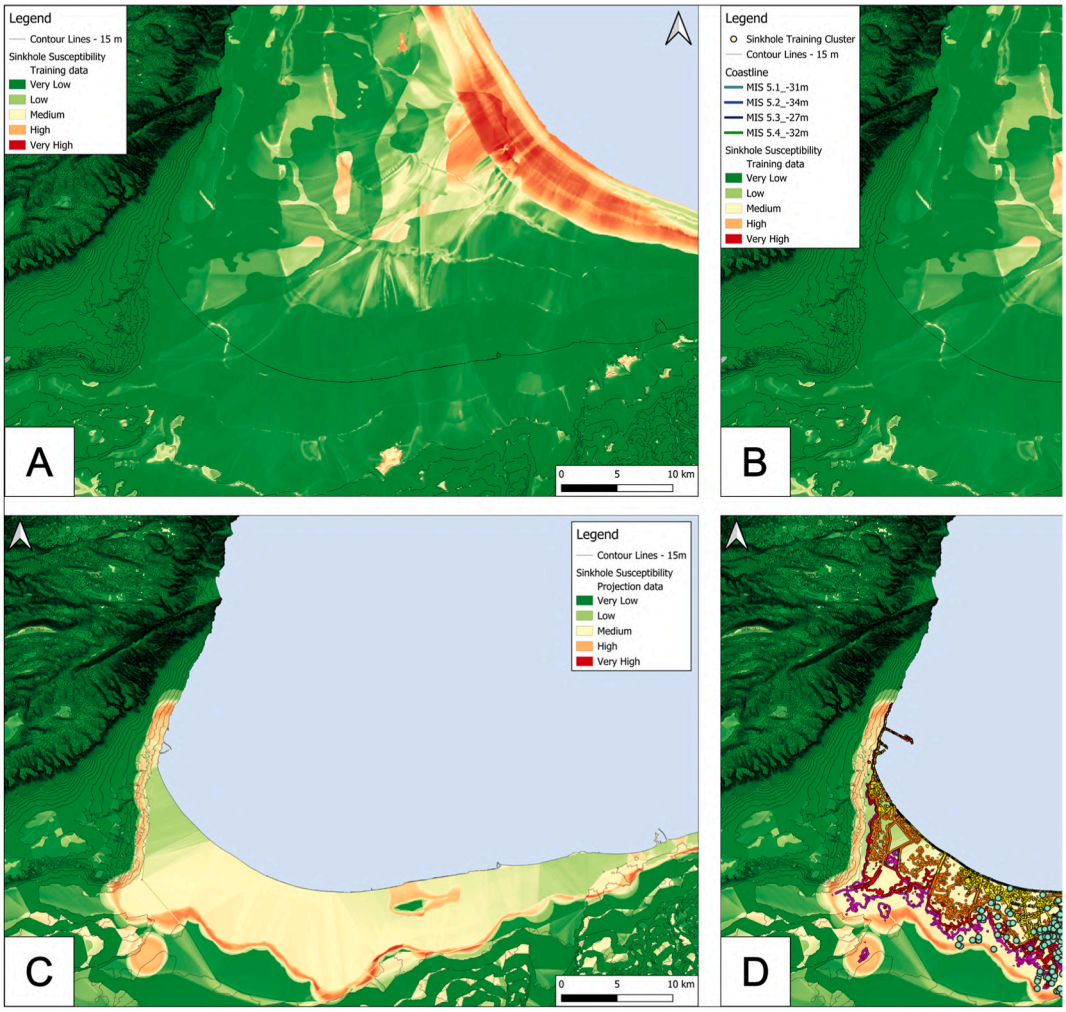

Fig. 12. Ensemble sinkhole susceptibility map. A and B refer to the training dataset, C and D to the projected dataset.

of land-use functionality.

5.3.2. Machine learning-based sinkholes susceptibility assessment

The machine learning workflow was structured into the phases of model training and simulation/prediction. In the first phase, a sinkhole susceptibility map was developed for a past time period, while in the second the trained model was applied to project future susceptibility under evolving coastal conditions. An ensemble modeling approach was adopted by integrating three established algorithms: Random Forest (RF) [104], Gradient Boosting Machines (GBM) [105], and Maximum Entropy (MaxEnt) [106]. This ensemble technique enhanced predictive robustness by combining the strengths of individual algorithms into a unified output.

The model incorporated several predisposing factors influencing sinkhole occurrence [107,108]: (1) overburden thickness, (2) lithology, (3) Relative Slope Position (RSP), (4) slope, (5) Topographic Wetness Index (TWI), and (6) coastline density, representing areas most affected by shoreline variation.

The training phase referred to the MIS 5, during which shoreline positions were reconstructed based on known sea-level oscillations, whereas the projection phase employed the SSP5–8.5 climate scenario for the years 2050, 2100, 2150, and 2175. Two independent sinkhole inventories, each corresponding to a distinct coastal city, were used respectively for training and validation phases (Fig. 11).

Model performance was assessed through the Receiver Operating Characteristic (ROC) curve and the Area Under the Curve (AUC) metric [109].

Variable importance quantified the contribution of each predisposing factor to predictive accuracy, expressed as the percentage loss in performance upon its exclusion. Among the predictors, coastline density, lithology and slope emerged as the most influential. Response curves demonstrated that increasing coastline density correlates positively with sinkhole susceptibility, while higher slope gradients reduce it. Intermediate coastline density values exhibited the greatest influence, and carbonate lithologies (class 2) were

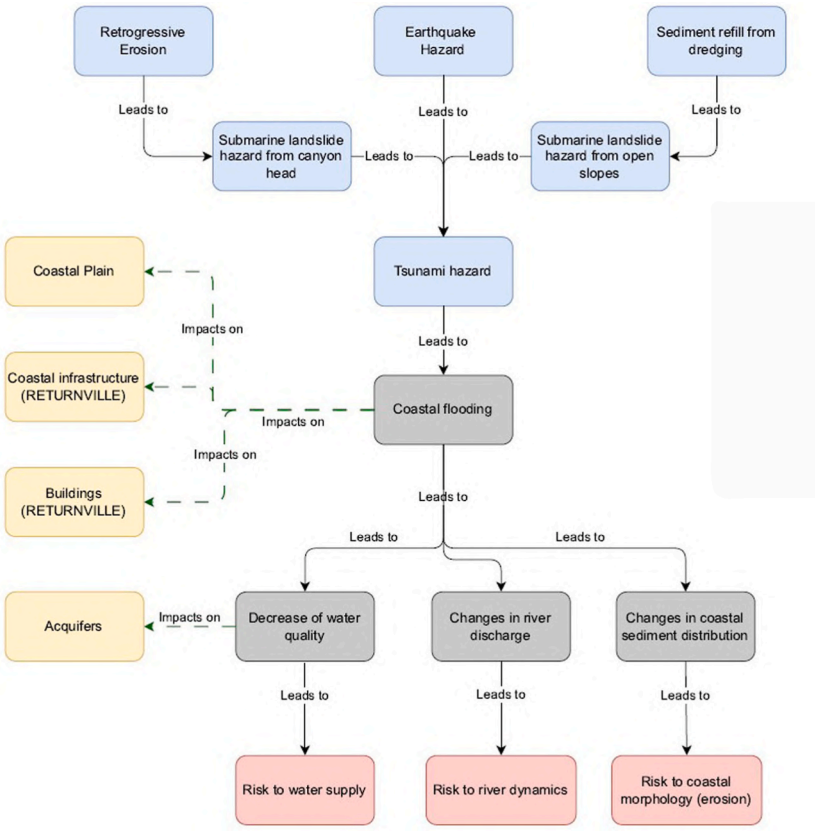

Fig. 13. Impact chain related to Coastal Flooding with hazard, impact and risk levels indicated as well as possible inferences of the climatic factor.

associated with higher susceptibility than clastic or magmatic rocks. Furthermore, low RSP values, corresponding to low-lying footslope areas, also indicated increased susceptibility, consistent with the role of gentle topographic gradients highlighted by the response curve for slope. The outputs of individual models generated during training (Fig. 12A–B) were adapted for projection datasets, resulting in predictive susceptibility scenarios aligned with the SSP5–8.5 coastal projections (Fig. 12C–D). The final ensemble sinkhole susceptibility map integrated these outputs into a consolidated predictive product.

The ensemble model demonstrated excellent predictive accuracy for the training dataset (ROC/AUC = 0.978) and very good performance for the 2175 projection under the SSP5–8.5 scenario (ROC/AUC = 0.865) [110].

6. Applicative perspectives

The digital ecosystem represented by RETURNLAND can be used as a demonstrator of effectiveness in the combination of tools that, starting from the definition of the geohazards, lead to the quantification of damage and, therefore, to a risk estimate, thus testing the applicability of the "impact chains" approach as defined in the literature [111–113]. Strictly speaking, impact chains should be understood here as logical-functional tools capable of converting the co-causality of natural processes into structural (damage) and anthropogenic (socio-economic resilience) relational effects in extended territorial contexts part of which can be referred to the virtual test beds dealing with urban areas (RETURNVILLEs) developed in the RETURN project framework as well.

This level of management allows the modulation of causative actions and the consequent possibility to weigh their effects in terms of resulting risk, as well as their scalability in both space and time. It represents the modulation of the cause-effect relationship expressed by impact chains that makes them effective for risk mitigation strategies and increased resilience. Indeed, having the possibility to scale the extent of the expected effects on an area achieves the objective of tailoring structural interventions and strategic solutions (including administrative and political ones) to the potentially vulnerable territory and its communities.

The level of vulnerability has not been explicitly reported in the impact chains considered here, as it is attributed to the urban and infrastructure element (RETURNVILLE), which implicitly contains it. Nonetheless, from a more inclusive perspective on impact logic, the territory itself and the related environment should be considered a vulnerable element, both in terms of geomorphological systems and biological ecosystems.

Furthermore, it should be remarked that the impact chains conceptualized here may or may not be triggered by climate-related forces and their potential variations. Therefore, co-causative conditions related to climate and other conditions cannot be considered upstream of the modeled chain of effects.

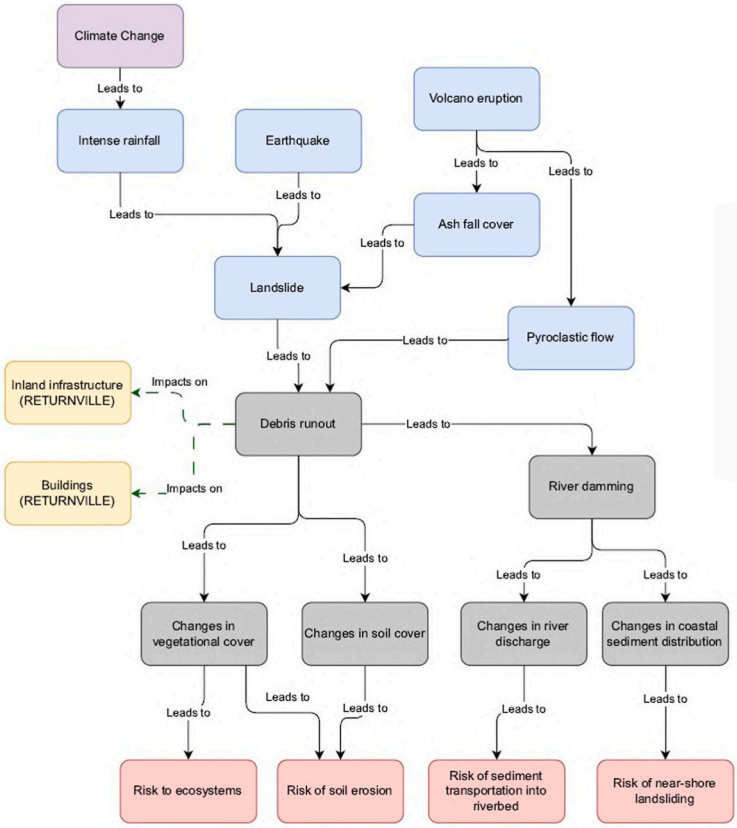

Fig. 14. Impact chain related to Landslide with hazard, impact and risk levels indicated as well as possible inferences of the climatic factor.

In relation to the tool chains considered in this study, three impact chains were derived respectively for Coastal Flooding (Fig. 13), Landslides (Fig. 14) and Settlements (Fig. 15).

Following the Coastal Flooding impact chain (Fig. 13), this study demonstrated, using quantitative effect analysis tools, the reproducibility in the RETURNLAND of part of the impact chain starting from a Submarine Landslide generated on a submerged open slope and canyon head that can cause a tsunami which impacts a coastal plain, inducing potential effects on water quality in aquifers, solid and liquid river flows, and coastal sediment distribution. In the demonstration exemplified here, the landslide is not explicitly generated by a specific cause but, for example, could be considered earthquake-induced or caused by human activities near the coast. Similarly, the origin of the tsunamigenic landslide could be considered to be a detachment of debris from an open slope caused by sediment redistribution (even of anthropogenic origin) due to refill from dredging.

Following the scheme shown in Fig. 14 related to the Landslide impact chain, this study demonstrated, using quantitative impact analysis tools, the reproducibility of part of the impact chain in the RETURNLAND starting from the effect of ash deposited during a volcanic eruption that modifies the debris cover on the reliefs, as a factor predisposing the possible triggering of shallow landslides by rainfall and/or earthquakes. The propagation of debris generated by landslides (both in the form of channeled flows and in open slope movements) can impact the slopes themselves, the debris flow channels and the rivers causing damming as well as can damage the plains present in the valley floors, impacting on vegetation cover, soil erosion, disturbance of fluvial dynamics and, consequently, the solid transport of sediments to the coast.

Finally, following the scheme reported in Fig. 15 related to the Settlement impact chain, in this study it was demonstrated, through quantitative effect analysis tools, the reproducibility in RETURNLAND of part of the impact chain starting from the climatic variation of the sea level (net of isostasy and regional subsidence, both natural and anthropogenic) which can induce variations in the coastline and determine the development of a coastal strip more vulnerable to the generation of sinkholes, whose impact can manifest itself in the variation of local water conditions and in the distribution of sediments, generating, in the latter case, a subsidence that in turn impacts on infrastructures or human settlements.

7. Conclusions

The construction of RETURNLAND as a virtual space, capable of representing the physiographic and morphodynamic characteristics of the Italian territory, was implemented within the PNRR-RETURN project, experimenting with a complex workflow to achieve a

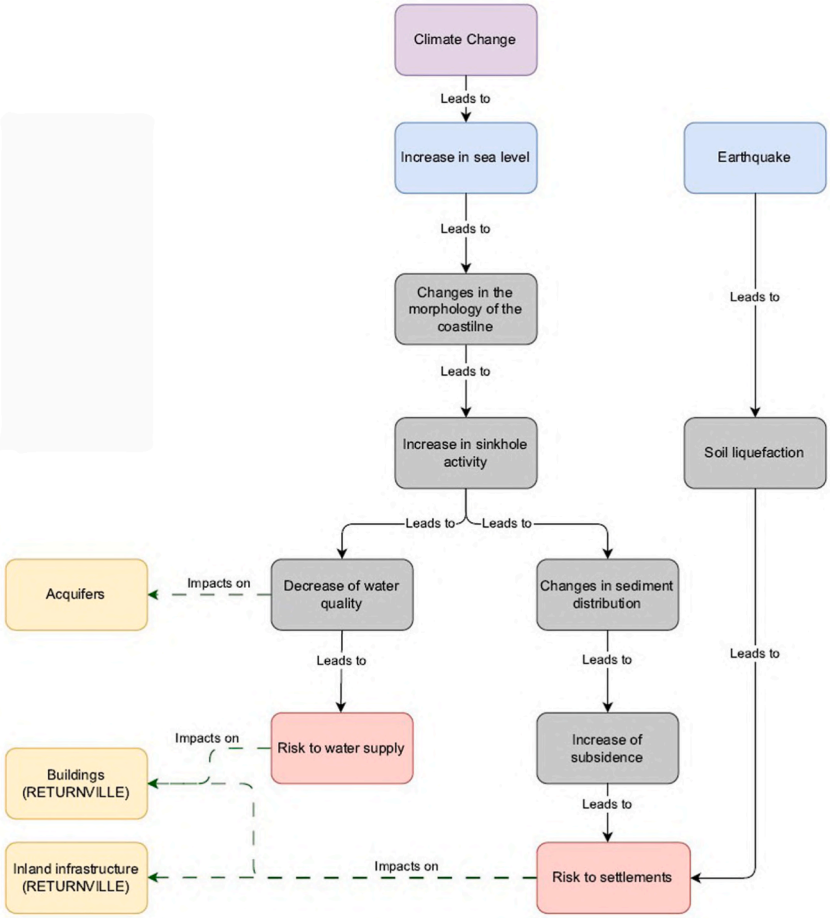

Fig. 15. Impact chain related to Settlement with hazard, impact and risk levels indicated as well as possible inferences of the climatic factor.

sustainable and meaningful integration of territorial elements. This respects fundamental physiographic constraints (such as drainage patterns, coastal development, contiguity of reliefs and plains), while ensuring the territorial scalability of the representations.

Through the deduction of impact chains, operational tools were exemplified at the scale of the physiographic unit, i.e., capable of representing effects involving multiple geomorphological contexts (e.g., nearshore and coastal plains, volcanoes and adjacent plains, hills and plains, coastal plateaus and nearshore), creating cascading impact scenarios.

The various tools, when considered individually, are the result of validation experiments on real cases, some of which had already been addressed prior to the RETURN project. However, when combined, they are able to demonstrate their effectiveness through an output-to-input functional logic, which has been demonstrated in this study by simulating the restitution of effects under three different conditions: i) a tsunami generated by a submarine landslide, the final effect of which translates into flooding of the coastal plain; ii) a volcanic eruption that simultaneously causes the ash deposition on the existing topography (predisposing to shallow landslide phenomena) and the direct impact on buildings of pyroclastic flows with determinable dynamic pressures and temperature; iii) widespread and concentrated subsidence within a coastal strip subject to sea level fluctuations over the last 120,000 years.

The methodological approach reported here offers, with RETURNLAD, to the scientific community an original training and analysis digital ecosystem for quantification of effect scenarios which, in itself, represents the first experiment in virtualization of a composite territory, starting from real physiographic conditions, never managed and never proposed at an international level. The prospect of using RETURNLAND in combination with other virtual test beds, such as those related to urban environments or infrastructures, as well as Digital Twins, expresses the potential of this product developed within the RETURN project. This potential is also evident in the context of hybrid training approaches for machine learning analysis aimed at developing artificial intelligence systems that are useful for designing strategies to increase resilience, with respect to scenarios of changing conditions surrounding natural systems, including a changing climate.

CRediT authorship contribution statement

Isabella Serena Liso: Writing – original draft, Methodology, Data curation, Conceptualization. **Rita Tufano:** Writing – original

draft, Visualization, Software, Methodology, Formal analysis, Data curation. **Giovanni Poneti:** Writing – original draft, Software, Methodology, Investigation, Formal analysis, Data curation. **Elena Scacchia:** Writing – original draft, Software, Methodology, Data curation, Conceptualization. **Rosa Colacicco:** Writing – review & editing, Writing – original draft, Visualization, Software, Methodology, Investigation, Data curation, Conceptualization. **Valeria Lo Presti:** Writing – review & editing, Writing – original draft, Software, Methodology, Formal analysis, Data curation, Conceptualization. **Giuseppe Bausilio:** Visualization, Software, Formal analysis, Data curation. **Silvia Massaro:** Writing – original draft, Software, Formal analysis. **Francesco Neglia:** Writing – original draft, Software, Investigation, Formal analysis. **Giovanni Scardino:** Writing – original draft, Visualization, Software, Formal analysis, Data curation. **Filippo Zaniboni:** Writing – original draft, Software, Investigation, Formal analysis. **Mariano Di Napoli:** Writing – original draft, Software. **Alberto Laurenti:** Writing – original draft, Software. **Domenico Calcaterra:** Writing – review & editing, Supervision, Funding acquisition. **Silvia Ceramicola:** Writing – review & editing, Writing – original draft, Supervision, Data curation, Conceptualization. **Francesco Latino Chiocci:** Writing – review & editing, Validation, Supervision, Resources, Methodology. **Pierfrancesco Dellino:** Writing – review & editing, Supervision. **Mario Parise:** Writing – review & editing, Supervision, Conceptualization. **Attilio Sulli:** Writing – review & editing, Supervision, Data curation. **Salvatore Martino:** Writing – review & editing, Writing – original draft, Supervision, Project administration, Funding acquisition, Conceptualization.

Funding sources

Research performed in the framework of the project 'RETURN Extended Partnership' and received funding from the European Union Next-Generation EU (National Recovery and Resilience Plan—NRRP, Mission 4, Component 2, Investment 1.3—D.D. 1243 2/8/2022) PE0000005.

Declaration of competing interest

The authors declare that they have no known competing financial interests or personal relationships that could have appeared to influence the work reported in this paper.

Data availability

The complete version of RETUNLAND is publicly available and can be downloaded from the Zenodo repository (https://doi.org/10.5281/zenodo.18987490) within the "RETURN Project – PNRR" community (https://zenodo.org/communities/return_pnrr).

References

[1] Fondazione Return. https://www.fondazionereturn.it/. (Accessed 25 October 2025).
[2] S. Martino, M. Della Seta, C. Esposito (Eds.), Geohazards and Disasters: Modelling Scenarios as a Challenge for the Future, Elsevier, Amsterdam, 2025, https://doi.org/10.1016/C2023-0-00231-X, 2025.
[3] M. Berti, F. Bozzano, D. Calcaterra, S. Ceramicola, G. Ciccarese, R. Colacicco, D. Di Martire, C. Esposito, R. Fanti, G. Forte, I.S. Liso, S. Martino, M. Parise, C. Tacconi Stefanelli, V. Tofani, Ground instability processes in the Italian territory: outcomes for advanced susceptibility methods from a national review of learning examples, in: Progress in Landslide Research and Technology, vol. 4, issue 2, Springer, Cham, 2025.
[4] A. Tadini, S. Massaro, A. Bevilacqua, P. Tierz, A. Aravena, Uncertainty quantification in volcanology: observations, numerical modelling, and hazard/risk assessment: preface to the special issue, Bull. Volcanol. 87 (6) (2025) 48, https://doi.org/10.1007/s00445-025-01835-y.
[5] H. Zhang, D. Ge, J. Liu, Y. Zhang, Multifunctional cyber-physical system testbed based on a source-grid combined scheduling control simulation system, IET Gener. Transm. Distrib. 11 (12) (2017) 3144–3151, https://doi.org/10.1049/iet-gtd.2016.1853.
[6] J. Reitz, D. Böken, J. Roßmann, A virtual testbed for the development and verification of cyber-physical systems, in: 2023 Winter Simulation Conference (WSC), IEEE, 2023, pp. 2837–2848, https://doi.org/10.1109/WSC60868.2023.10407609.
[7] Y. Sun, J. Tu, M. Bragin, L. Zhang, A simulation-based integrated virtual testbed for dynamic optimization in smart manufacturing systems, J. Adv. Manuf. Sci. Process 4 (4) (2022) e10141, https://doi.org/10.1002/amp2.10141.
[8] Y.A. Nanehkaran, Z. Licai, J. Chen, M. Azarafza, M. Yimin, Application of artificial neural networks and geographic information system to provide hazard susceptibility maps for rockfall failures, Environ. Earth Sci. 81 (19) (2022) 475, https://doi.org/10.1007/s12665-022-10603-6.
[9] M. Meyer, T. Farei-Campagna, A. Pasztor, R.D. Forno, T. Gsell, J. Faillettaz, A. Vieli, S. Weber, J. Beutel, L. Thiele, Event-triggered natural hazard monitoring with convolutional neural networks on the edge, in: Proceedings of the 18th International Conference on Information Processing in Sensor Networks, 2019, pp. 73–84, https://doi.org/10.1145/3302506.3310390.
[10] M. Meyer, S. Weber, J. Beutel, L. Thiele, Systematic identification of external influences in multi-year microseismic recordings using convolutional neural networks, Earth Surf. Dyn. 7 (1) (2019) 171–190, https://doi.org/10.5194/esurf-7-171-2019.
[11] A. Moeineddin, C. Seguí, S. Dueber, R. Fuentes, Physics-informed neural networks applied to catastrophic creeping landslides, Landslides 20 (9) (2023) 1853–1863, https://doi.org/10.1007/s10346-023-02072-0.
[12] M. Javaid, A. Haleem, R. Suman, Digital twin applications toward industry 4.0: a review, Cognit. Rob. 3 (2023) 71–92, https://doi.org/10.1016/j.cogr.2023.04.003.
[13] S.A. Enderami, E.J. Sutley, R.K. Mazumder, M. Dumler, Virtual testbeds for community resilience analysis: step-by-step development procedure and future orientation, Resilient Cities Struct 2 (2) (2023) 42–56, https://doi.org/10.1016/j.rcns.2023.07.002.
[14] M. Homaei, Ó. Mogollón-Gutiérrez, J.C. Sancho, M. Ávila, A. Caro, A review of digital twins and their application in cybersecurity based on artificial intelligence, Artif. Intell. Rev. 57 (8) (2024) 201, https://doi.org/10.1007/s10462-024-10805-3.
[15] P.R. Federici, La varietà dei paesaggi naturali, in: Touring Club Italiano (Ed.), Il Paesaggio Italiano, Touring Editore, Milano, 2000, pp. 11–26, 2000.
[16] M. Marchetti, M. Soldati, V. Vandelli, The great diversity of Italian landscapes and landforms: their origin and human imprint, in: M. Soldati, M. Marchetti (Eds.), Landscapes and Landforms of Italy. World Geomorphological Landscapes, Springer, Cham, 2017, pp. 7–20, https://doi.org/10.1007/978-3-319-26194-2_2.
[17] S. Fratianni, F. Acquaotta, The climate of Italy, in: M. Soldati, M. Marchetti (Eds.), Landscapes and Landforms of Italy, Springer, Cham, 2017, pp. 29–38, https://doi.org/10.1007/978-3-319-26194-2_2.

[18] F. Santucci de Magistris, G. Lanzano, G. Forte, G. Fabbrocino, A peak acceleration threshold for soil liquefaction: lessons learned from the 2012 Emilia earthquake Italy, Nat. Hazards 74 (2) (2014) 1069–1094, https://doi.org/10.1007/s11069-014-1229-x.

[19] P. Fredi, E. Lupia Palmieri, Morphological regions of Italy, in: M. Soldati, M. Marchetti (Eds.), Landscapes and Landforms of Italy. World Geomorphological Landscapes, Springer, Cham, 2017, pp. 39–74, https://doi.org/10.1007/978-3-319-26194-2_5.

[20] R. Catalano, C. Doglioni, S. Merlini, On the Mesozoic Ionian basin, Geophys. J. Int. 144 (1) (2001) 49–64, https://doi.org/10.1046/j.0956-540X.2000.01287.x.

[21] S. Ceramicola, D. Praeg, M. Coste, E. Forlin, A. Cova, E. Colizza, S. Critelli, Submarine mass-movements along the slopes of the active Ionian continental margins and their consequences for marine geohazards (Mediterranean Sea), in: Krastel, et al. (Eds.), Submarine Mass Movements and Their Consequences: 6Th International Symposium Advances in Natural and Technological Hazards Research, vol. 26, Springer Science + Business Media B.V. Ch., 2014, pp. 295–306, https://doi.org/10.1007/978-3-319-00972-8_26.

[22] L. Guerrieri, V. Comerci, L. Ferreli, R. Pompili, L. Serva, F. Brunamonte, A. Michetti, Geological evolution of the intermountain Rieti basin (Central Appennines), in: Mapping Geology in Italy, vol 2004, SELCA, Firenze, 2004, pp. 123–130, 2006.

[23] C. Archer, P. Noble, M.R. Rosen, L. Sagnotti, F. Florindo, S. Mensing, G. Piovesan, A.M. Michetti, Lakes as paleoseismic records in a seismically-active, low-relief area (Rieti Basin, central Italy), Quat. Sci. Rev. 211 (2019) 186–207, https://doi.org/10.1016/j.quascirev.2019.03.004.

[24] E. Patacca, P. Scandone, M. Bellatalla, N. Perilli, U. Santini, The Numidian-sand event in the Southern Apennines, Mem. Sci. Geol. Padova 43 (1992) 297–337.

[25] D. Cosentino, M. Parotto, La struttura a falde della Sabina (Appennino centrale), in: M. Tozzi, G.P. Cavinato, M. Parotto (Eds.), Studi Preliminari All'Acquisizione Dati Del Profilo CROP 11 Civitavecchia-Vasto, Voi 1991/2. Studi Geologici Camerti, Università Degli Studi Di Camerino, 1992, pp. 381–387 (in Italian).

[26] C. Doglioni, Some remarks on the origin of the foredeeps, Tectonophysics 228 (1993) 1–20, https://doi.org/10.1016/0040-1951(93)90211-2.

[27] N. D'Agostino, J.A. Jackson, F. Dramis, R. Funiciello, Interactions between mantel upwelling, drainage evolution and active normal faulting: an example from the central Apennines Italy, Geophys. J. Int. 147 (2) (2001) 475–497, https://doi.org/10.1046/j.1365-246X.2001.00539.x.

[28] G.P. Cavinato, P.D. Celles, Extensional basins in the tectonically bimodal central Apennines fold-thrust belt, Italy: response to corner flow above a subducting slab in retrograde motion, Geology 27 (10) (1999) 955–958, https://doi.org/10.1130/0091-7613(1999)027%3C0955:EBITTB%3E2.3.CO;2.

[29] E. Cuoco, G. Verrengia, S. De Francesco, D. Tedesco, Hydrogeochemistry of Roccamonfina volcano (southern Italy), Environ. Earth Sci. 61 (3) (2010) 525–538, https://doi.org/10.1007/s12665-009-0363-3.

[30] S. Conticelli, S. Marchionni, D. Rosa, G. Giordano, E. Boari, R. Avanzinelli, Shoshonite and sub-alkaline magmas from an ultrapotassic volcano: Sr–Nd–Pb isotope data on the Roccamonfina volcanic rocks, Roman Magmatic Province, Southern Italy, Contrib. Mineral. Petrol. 157 (1) (2009) 41–63, https://doi.org/10.1007/s00410-008-0319-8.

[31] G. Scardino, M. Anzidei, P. Petio, E. Serpelloni, V. De Santis, A. Rizzo, S.I. Liso, M. Zingaro, D. Capolongo, A. Vecchio, A. Refice, G. Scicchitano, The impact of future sea-level rise on low-lying subsiding coasts: a case study of Tavoliere delle puglie (Southern Italy), Remote Sens. 14 (19) (2022) 4936, https://doi.org/10.3390/rs14194936.

[32] V. De Santis, M. Caldara, L. Pennetta, T. Torres, J.E. Ortiz, Unconformity-bounded stratigraphic units (UBSUs) in an Italian alluvial-plain area: recognizing and dating. J. Sediment, Res. 83 (1) (2013) 96–113, https://doi.org/10.2110/jsr.2013.7.

[33] R. Colacicco, A. Refice, R. Nutricato, F. Bovenga, G. Caporusso, A. D'Addabbo, M. La Salandra, F.P. Lovergine, D.O. Nitti, D. Capolongo, High-resolution flood monitoring based on advanced statistical modeling of Sentinel-1 multi-temporal stacks, Remote Sens. 16 (2) (2024) 294, https://doi.org/10.3390/rs16020294.

[34] I. Lapietra, R. Colacicco, A. Rizzo, D. Capolongo, Mapping social vulnerability to multi-hazard scenarios: a GIS-based approach at the census tract level, Appl. Sci. 14 (11) (2024) 4503, https://doi.org/10.3390/app14114503.

[35] A. Aiello, F. Canora, G. Pasquariello, G. Spilotro, Shoreline variations and coastal dynamics: a space–time data analysis of the Jonian littoral, Italy, Estuar. Coast Shelf Sci. 129 (2013) 124–135, https://doi.org/10.1016/j.ecss.2013.06.012.

[36] D. Gioia, M. Bavusi, P. Di Leo, T. Giammatteo, M. Schiattarella, Geoarchaeology and geomorphology of the Metaponto area, Ionian coastal belt, Italy, J. Maps 16 (2) (2020) 117–125, https://doi.org/10.1080/17445647.2019.1701575.

[37] A. Fabbri, F. Ghisetti, L. Vezzani, The Peloritani-Calabria range and the Gioia basin in the Calabrian arc (Southern Italy): relationships between land and marine data, Geol. Rom. 19 (1980) 131–150, 1980.

[38] F. Antonioli, L. Ferranti, K. Lambeck, S. Kershaw, V. Verrubbi, G. Dai Pra, Late Pleistocene to Holocene record of changing uplift rates in southern Calabria and northeastern Sicily (southern Italy, Central Mediterranean Sea), Tectonophysics 422 (2006) 23–40, https://doi.org/10.1016/j.tecto.2006.05.003, 2006.

[39] D. Casalbore, A. Bosman, D. Casas, F. Chiocci, E. Martorelli, D. Ridente, Morphological variability of submarine mass movements in the tectonically–controlled Calabro–Tyrrhenian Continental Margin (Southern Italy), Geosciences 9 (1) (2019) 43, https://doi.org/10.3390/geosciences9010043.

[40] S A. Cova Ceramicola, E. Forlin, N. Markezic, G. Mangano, D. Civile, M. Zecchin, F. Fanucci, E. Colizza, C. Corselli, D. Morelli, A. Savini, A. Caburlotto, O. Candoni, M. Coste, D. Cotterle, S. Critelli, A. Cuppari, M. Deponte, R. Dominici, L. Facchin, E. Gordini, M. Locatelli, F. Muto, D. Praeg, R. Romeo, C. Tessarolo, Geohazard features of the Ionian Calabrian margin, J. Maps 20 (1) (2024) 2349785, https://doi.org/10.1080/17445647.2024.2349785.

[41] F.L. Chiocci, F. Budillon, S. Ceramicola, F.G. Orrù, Atlante Dei Lineamenti Di Pericolosità Geologica Dei Mari italiani-Risultati Del Progetto Magic (2021), CNR edizioni, 2021, p. 350, 978-88-8080-457-4.

[42] M. Bianchini, F.L. Chiocci, S. Ceramicola, A submarine landslides database of Calabrian Continental margins (Central Mediterranean Sea), Sci. Data 12 (2025), https://doi.org/10.1038/s41597-025-06239-3, 1951.

[43] C. Lo Iacono, A. Sulli, M. Agate, V. Lo Presti, F. Pepe, R. Catalano, Submarine canyons and slope failures in the Palermo Gulf (Southern Tyrrhenian Sea): implications for geo-hazard assessment, Mar. Geophys. Res. (2011), https://doi.org/10.1007/s11001-011-9118-0.

[44] A. Sulli, M. Agate, C.L. Iacono, V.L. Presti, V. Pennino, S. Polizzi, Submarine slope failures along the northern Sicilian continental margin (Southern Tyrrhenian Sea) and possible implications for geo-hazard, in: Landslide Science and Practice vol. 5, Springer Berlin Heidelberg, Berlin, Heidelberg, 2013, pp. 41–48, https://doi.org/10.1007/978-3-642-31427-8_5.

[45] M. Polese, G. Tocchi, M.F. Clemente, B. Di Palma, M. Gaetani d'Aragona, D. Molinari, G. Treglia, L. Lavalle, C. Bragalli, L.C. Zingali, G. Freni, S. Piazza, M. Pittore, A. Pirni, A.M. Zaccaria, C. Arrighi, M. Losasso, A. Prota, Virtual testbed for multi-risk assessment: defining RETURNVILLEs to support the analysis and testing of DRM and CCA solutions in realistic urban contexts, Int. J. Disaster Risk Reduct. (2026) submitted for publication.

[46] Tinitaly DEM. https://tinitaly.pi.ingv.it/. (Accessed 25 October 2025).

[47] S. Tarquini, I. Isola, M. Favalli, F. Mazzarini, M. Bisson, M.T. Pareschi, E. Boschi, TINITALY/01: a new triangular irregular network of Italy, Ann. Geophys. 50 (3) (2007) 407–425, https://doi.org/10.4401/ag-4424.

[48] S. Tarquini, S. Vinci, M. Favalli, F. Doumaz, A. Fornaciai, L. Nannipieri, Release of a 10-m-resolution DEM for the Italian territory: comparison with global-coverage DEMs and anaglyph-mode exploration via the web, Comput. Geosci. 38 (1) (2012) 168–170, https://doi.org/10.1016/j.cageo.2011.04.018.

[49] S. Tarquini, L. Nannipieri, The 10 m-resolution TINITALY DEM as a trans-disciplinary basis for the analysis of the Italian territory: current trends and new perspectives, Geomorphology 281 (2017) 108–115, https://doi.org/10.1016/j.geomorph.2016.12.022.

[50] Geoportale - Regione Emilia-Romagna. https://geoportale.regione.emilia-romagna.it (last access on 25 October 2025).

[51] S.I.T. - Puglia.con. https://pugliacon.regione.puglia.it/web/sit-puglia-sit. (Accessed 25 October 2025).

[52] RSDI Basilicata- GeoPortale. https://rsdi.regione.basilicata.it/. (Accessed 25 October 2025).

[53] EMODnet Digital Bathymetry, EMODnet Bathymetry consortium. https://doi.org/10.12770/cf51df64-56f9-4a99-b1aa-36b8d7b743a1, DTM 2024.

[54] Blue Marble Geographics, Global mapper [Software], https://www.bluemarblegeo.com/global-mapper/, 2025. (Accessed 25 October 2025).

[55] Esri, ArcGIS pro [Software]. https://www.esri.com/software/arcgis-pro, 2025. (Accessed 25 October 2025).

[56] S. Martino, M. Polese, A. Prota, Digital ecosystem: RETURNLAND and RETURNVILLES (Version V1), Zenodo (2026), https://doi.org/10.5281/zenodo.18987490 [Data set].

[57] "RETURN Project – PNRR" Zenodo Community. https://zenodo.org/communities/return_pnrr, 2026. (Accessed 10 March 2026).

[58] ISTAT, Rapporto Sul Territorio, 2020, https://doi.org/10.1481/Istat.Rapportoterritorio.2020.
[59] S. Massaro, M. Stocchi, B. Martínez Montesinos, L. Sandri, J. Selva, R. Sulpizio, B. Giaccio, M. Moscatelli, E. Peronace, M. Nocentini, R. Isaia, M. Titos Luzón, P. Dellino, G. Naso, A. Costa, Assessing long-term tephra fallout hazard in southern Italy from Neapolitan volcanoes, Nat. Hazards Earth Syst. Sci. 23 (2023) 2289–2311, https://doi.org/10.5194/nhess-23-2289-2023, 2023.
[60] A. Folch, L. Mingari, N. Gutierrez, M. Hanzich, G. Macedonio, A. Costa, FALL3D-8.0: a computational model for atmospheric transport and deposition of particles, aerosols and radionuclides – part 1: model physics and numerics, Geosci. Model Dev. (GMD) 13 (2020) 1431–1458, https://doi.org/10.5194/gmd-13-1431-2020.
[61] A. Costa, A. Folch, G. Macedonio, Density-driven transport in the umbrella region of volcanic clouds: impications for tephra dispersion models, Geophys. Res. Lett. 40 (2013) 4823–4827, https://doi.org/10.1002/grl.50942.
[62] H. Hersbach, B. Bell, P. Berrisford, S. Hirahara, A. Horányi, J. Muñoz-Sabater, C. Peubey, R. Radu, D. Schepers, A. Simmons, C. Soci, S. Abdalla, X. Abellan, G. Balsamo, P. Bechtold, G. Biavati, J. Bidlot, M. Bonavita, G. De Chiara, P. Dahlgren, D. Dee, M. Diamantakis, R. Dragani, J. Flemming, R. Forbes, M. Fuentes, A. Geer, L. Haimberger, S. Healy, R.J. Hogan, E. Hólm, M. Janisková, S. Keeley, P. Laloyaux, P. Lopez, C. Lupu, G. Radnoti, P. de Rosnay, I. Rozum, F. Vamborg, S. Villaume, J.N. Thépaut, The ERA5 global reanalysis, Q. J. R. Meteorol. Soc. 146 (730) (2020) 1999–2049, https://doi.org/10.1002/qj.3803.
[63] L. Sandri, A. Costa, J. Selva, R. Tonini, G. Macedonio, A. Folch, R. Suplizio, Beyond eruptive scenarios: assessing tephra fallout hazard from Neapolitan volcanoes, Sci. Rep. 6 (2016) 24271, https://doi.org/10.1038/srep24271.
[64] B.M. Montesinos, M.T. Luzón, L. Sandri, O. Rudyy, A. Cheptsov, G. Macedonio, A. Folch, S. Barsotti, J. Selva, A. Costa, On the feasibility and usefulness of high-performance computing in probabilistic volcanic hazard assessment: an application to tephra hazard from Campi Flegrei, Front. Earth Sci. 10 (2022) 941789, https://doi.org/10.3389/feart.2022.941789.
[65] S. de Vita, G. Orsi, L. Civetta, A. Caradente, M. D'Antonio, A.L. Deino, T. di Cesare, M.A. di Vito, R.V. Fisher, R. Isaia, E. Marotta, A. Necco, M.H. Ort, L. Pappalardo, M. Piochi, J.R. Southon, The Agnano-Monte Spina eruption (4100 years BP) in the restless Campi Flegrei caldera Italy, J. Volcanol. Geoth. Res. 91 (1999) 269–301, https://doi.org/10.1016/S03770273(99)00039-6, 1999.
[66] P. Dellino, F. Dioguardi, D.M. Doronzo, D. Mele, The rate of sedimentation from turbulent suspension: an experimental model with application to pyroclastic density currents and discussion on the grain-size dependence of flow runout, Sedimentology 66 (1) (2019) 129–145, https://doi.org/10.1111/sed.12485.
[67] G. Lube, E.C. Breard, T. Esposti-Ongaro, J. Dufek, B. Brand, Multiphase flow behaviour and hazard prediction of pyroclastic density currents, Nat. Rev. Earth Environ. 1 (7) (2020) 348–365, https://doi.org/10.1038/s43017-020-0064-8.
[68] P. Dellino, F. Dioguardi, R. Isaia, R. Sulpizio, D. Mele, The impact of pyroclastic density currents duration on humans: the case of the AD 79 eruption of Vesuvius, Sci. Rep. 11 (1) (2021) 4959, https://doi.org/10.1038/s41598-021-84456-7.
[69] P. Dellino, D. Mele, R. Sulpizio, L. La Volpe, G. Braia, A method for the calculation of the impact parameters of dilute pyroclastic density currents based on deposit particle characteristics, J. Geophys. Res. Solid Earth 113 (B7) (2008), https://doi.org/10.1029/2007JB005365.
[70] G.A. Valentine, Initiation of dilute and concentrated pyroclastic currents from collapsing mixtures and origin of their proximal deposits, Bull. Volcanol. 82 (2) (2020), https://doi.org/10.1007/s00445-020-1366-x.
[71] R.A.F. Cas, J.V. Wright, Volcanic Successions: Modern and Ancient. A Geological Approach to Processes, Products and Successions, Allen and Unwin, London, 1987, pp. 1–518, https://doi.org/10.1007/978-94-009-3167-1.
[72] G.A. Valentine, Damage to structures by pyroclastic flows and surges, inferred from nuclear weapons effects, J. Volcanol. Geoth. Res. 87 (1–4) (1998) 117–140, https://doi.org/10.1016/S0377-0273(98)00094-8.
[73] D.M. Doronzo, P. Dellino, Interaction between pyroclastic density currents and buildings: numerical simulation and first experiments, Earth Planet Sci. Lett. 310 (3-4) (2011) 286–292, https://doi.org/10.1016/j.epsl.2011.08.017.
[74] ANSYS, Inc, ANSYS Fluent [Software], https://www.ansys.com/products/fluids/ansys-fluent, 2025. (Accessed 25 October 2025).
[75] F. Neglia, R. Sulpizio, F. Dioguardi, D. Sarocchi, Investigating the effect of polydispersity on the dynamics of multiphase flows using computational fluid dynamics tools, Int. J. Multiphas. Flow 168 (2023) 104558, https://doi.org/10.1016/j.ijmultiphaseflow.2023.104558.
[76] G.A. Valentine, K.H. Wohletz, Numerical models of Plinian eruption columns and pyroclastic flows, J. Geophys. Res. 94 (B2) (1989) 1867–1887, https://doi.org/10.1029/JB094IB02P01867.
[77] F. Dobran, A. Neri, G. Macedonio, Numerical simulation of collapsing volcanic columns, J. Geophys. Res. 98 (B3) (1993) 4231–4259, https://doi.org/10.1029/92JB02409.
[78] A. Neri, T. Esposti Ongaro, G. Macedonio, D. Gidaspow, Multiparticle simulation of collapsing volcanic columns and pyroclastic flow, J. Geophys. Res. Solid Earth 108 (B4) (2003) 2202, https://doi.org/10.1029/2001JB000508.
[79] S. Dartevelle, W.I. Rose, J. Stix, K. Kelfoun, J.W. Vallance, Numerical modeling of geophysical granular flows: 2. Computer simulations of plinian clouds and pyroclastic flows and surges, G-cubed 5 (8) (2004) 8004, https://doi.org/10.1029/2003GC000637.
[80] J. Dufek, G.W. Bergantz, Suspended load and bed-load transport of particle-laden gravity currents: the role of particle-bed interaction, Theor. Comput. Fluid Dynam. 21 (2) (2007) 119–145, https://doi.org/10.1007/s00162-007-0041-6.
[81] A. Neri, T.E. Ongaro, G. Menconi, M. De', M. Vitturi, C. Cavazzoni, G. Erbacci, P.J. Baxter, E. Ongaro, G. Menconi, M. De', C. Cavazzoni, G. Erbacci, P.J. Baxter, 4D simulation of explosive eruption dynamics at Vesuvius, Geophys. Res. Lett. 34 (4) (2007) 4309, https://doi.org/10.1029/2006GL028597.
[82] T. Esposti Ongaro, A. Neri, G. Menconi, M. de'Michieli Vitturi, P. Marianelli, C. Cavazzoni, G. Erbacci, P.J. Baxter, Transient 3D numerical simulations of column collapse and pyroclastic density current scenarios at Vesuvius, J. Volcanol. Geoth. Res. 178 (3) (2008) 378–396, https://doi.org/10.1016/J.JVOLGEORES.2008.06.036.
[83] M. Cerminara, T. Esposti Ongaro, A. Neri, Large Eddy simulation of gas–particle kinematic decoupling and turbulent entrainment in volcanic plumes, J. Volcanol. Geoth. Res. 326 (2016) 143–171, https://doi.org/10.1016/J.JVOLGEORES.2016.06.018.
[84] R. Cioni, S. Levi, R. Sulpizio, Apulian Bronze Age Pottery as a long-distance Indicator of the Avellino Pumice Eruption (Vesuvius, Italy), Geological Society, London, Special Publications, 2000, https://doi.org/10.1144/GSL.SP.2000.171.01.13.
[85] S.B. Savage, K. Hutter, The motion of a finite mass of granular material down a rough incline, J. Fluid Mech. 199 (2697) (1989) 177–215, https://doi.org/10.1017/S0022112089000340.
[86] R.M. Iverson, The physics of debris flows, Rev. Geophys. 35 (3) (1997) 245–296, https://doi.org/10.1029/97RG00426.
[87] S.K. Chough, Y.K. Sohn, Depositional mechanics and sequences of base surges, Songaksan tuff ring, Cheju Island, Korea, Sedimentology 37 (6) (1990) 1115–1135, https://doi.org/10.1111/j.1365-3091.1990.tb01849.x.
[88] R. Sulpizio, D. Mele, P. Dellino, L. La Volpe, Deposits and physical properties of pyroclastic density currents during complex Subplinian eruptions: the AD 472 (Pollena) eruption of Somma-Vesuvius, Italy, Sedimentology 54 (3) (2007) 607–635, https://doi.org/10.1111/j.1365-3091.2006.00852.x.
[89] R. Sulpizio, P. Dellino, Chapter 2 sedimentology, depositional mechanisms and pulsating behaviour of pyroclastic density currents, Dev. Volcanol. 10 (C) (2008) 57–96, https://doi.org/10.1016/S1871-644X(07)00002-2.
[90] P.J. Baxter, A. Neri, M. Todesco, Physical modelling and human survival in pyroclastic flows, Nat. Hazards 17 (2) (1998) 163–176, https://doi.org/10.1023/A:1008031004183/METRICS.
[91] S. Glasstone, P.J. Dolan, The effects of nuclear weapons, US Dept. of Defense and Dept. of Energy (1977) 653.
[92] S. Ceramicola, S. Tinti, F. Zaniboni, D. Praeg, P. Planinsek, G. Pagnoni, E. Forlin, Reconstruction and tsunami modeling of a submarine landslide on the Ionian margin of Calabria (Mediterranean sea), in: Landslide Science for a Safer Geoenvironment: Volume 3: Targeted Landslides, 2014, pp. 557–562, https://doi.org/10.1007/978-3-319-04996-0_85.
[93] F. Zaniboni, G. Pagnoni, G. Gallotti, M.A. Paparo, A. Armigliato, S. Tinti, Assessment of the 1783 Scilla landslide–tsunami's effects on the Calabrian and Sicilian coasts through numerical modelling, Nat. Hazards Earth Syst. Sci. 19 (2019) 1585–1600, https://doi.org/10.5194/nhess-19-1585-2019.
[94] L. Gasperini, F. Zaniboni, A. Armigliato, S. Tinti, G. Pagnoni, M.S. Özeren, M. Ligi, F. Natali, a A. Poloni, Tsunami potential source in the eastern Sea of Marmara (NW Turkey), along the North Anatolian fault system, Landslides 19 (2022) 2295–2310, https://doi.org/10.1007/s10346-022-01929-0.

[95] G. Gallotti, F. Zaniboni, D. Arcangeli, C. Angeli, A. Armigliato, L. Cocchi, F. Muccini, M. Zanetti, S. Tinti, G. Ventura, The tsunamigenic potential of landslide-generated tsunamis on the Vavilov seamount, J. Volcanol. Geoth. Res. 434 (2023) 107745, https://doi.org/10.1016/j.jvolgeores.2023.107745.
[96] F. Zaniboni, G. Pagnoni, G. Gallotti, S. Tinti, A. Armigliato, Landslide-tsunamis along the flanks of Mount Epomeo, Ischia: propagation patterns and coastal hazard for the Campania coasts, in: Italy From, E. Marotta, L. D'Auria, F. Zaniboni, R. Nave (Eds.), Volcanic Island: from Hazard Assessment to Risk Mitigation, Geological Society, London, Special Publications, 2024, p. 519, https://doi.org/10.1144/SP519-2020-128.
[97] D. Casas, F. Chiocci, D. Casalbore, G. Ercilla, J.O. De Urbina, Magnitude-frequency distribution of submarine landslides in the Gioia Basin (southern Tyrrhenian Sea), Geo Mar. Lett. 36 (6) (2016) 405–414, https://doi.org/10.1007/s00367-016-0458-2.
[98] D.L. Kriebel, P.J. Lynett, D.T. Cox, C.M. Petroff, I.N. Robertson, G.Y. Chock, Energy method for approximating overland tsunami flows, J. Waterw. Port, Coast. Ocean Eng. 143 (5) (2017) 04017014, https://doi.org/10.1061/(ASCE)WW.1943-5460.0000393.
[99] C.J. Van der Sande, S.M. De Jong, A.P.J. De Roo, A segmentation and classification approach of IKONOS-2 imagery for land cover mapping to assist flood risk and flood damage assessment, Int. J. Appl. Earth Obs. Geoinf. 4 (3) (2003) 217–229, https://doi.org/10.1016/S0303-2434(03)00003-5.
[100] M. Parise, Sinkholes, subsidence and related mass movements, in: J.J.F. Shroder (Ed.), Treatise on Geomorphology, vol. 5, Elsevier, Academic Press, 2022, pp. 200–220, https://doi.org/10.1016/B978-0-12-818234-5.00029-8. ISBN: 9780128182345.
[101] F. Antonioli, L. Ferranti, P. Stocchi, G. Deiana, V. Lo Presti, S. Furlani, C. Marino, P. Orru, G. Scicchitano, E. Trainito, M. Anzidei, M. Bonamini, P. Sansò, G. Mastronuzzi, Morphometry and elevation of the last interglacial tidal notches in tectonically stable coasts of the Mediterranean Sea, Earth Sci. Rev. 185 (2018) 600–623, https://doi.org/10.1016/j.earscirev.2018.06.017.
[102] F. Antonioli, S. Furlani, P. Montagna, P. Stocchi, The use of submerged speleothems for sea level studies in the Mediterranean Sea: a new perspective using glacial isostatic adjustment (GIA), Geosciences 11 (2) (2021) 77, https://doi.org/10.3390/geosciences11020077.
[103] F. Antonioli, L. Ferranti, M. Agate, A. Ascione, C. Cerrone, V. De Santis, G. Deiana, A. Fontana, S. Furlani, G. Leoni, V. Lo Presti, L. Guerrieri, G. Mastronuzzi, C. Monaco, P. Orrù, P. Pieruccini, A. Sulli, The last interglacial transgression in Italy: the breath of the Italian coasts documented by 461 sites, Quat. Sci. Rev. 360 (2025), https://doi.org/10.1016/j.quascirev.2025.109376.
[104] L. Breiman, Random forests, Mach. Learn. 45 (1) (2001) 5–32, https://doi.org/10.1023/A:1010933404324. Kluwer Academic Publishers.
[105] J.H. Friedman, Greedy function approximation: a gradient boosting machine. Institute of mathematical statistics, Ann. Stat. 29 (5) (2001) 1189–1232, https://doi.org/10.1214/aos/1013203451.
[106] S.J. Phillips, M. Dudík, Modeling of species distributions with Maxent: new extensions and a comprehensive evaluation, Ecography 31 (2) (2008) 161–175, https://doi.org/10.1111/j.0906-7590.2008.5203.x.
[107] I.S. Liso, M. Parise, Sinkhole development at the freshwater-saltwater interface in Apulia (southern Italy), in: L. Land, C. Kromhout, S. Suter (Eds.), Proceedings of the 17th Multidisciplinary Conference on Sinkholes and the Engineering and Environmental Impacts of Karst, Tampa, Florida, USA, 2023, pp. 229–238, 27-31 March 2023, NCKRI Symposium no. 9.
[108] I.S. Liso, Sinkhole occurrence and evolution, and seawater intrusion in a low-coastal setting of Apulia, Ital. J. Eng. Geol. Environ. (2024) 197–204, https://doi.org/10.4408/IJEGE.2024-01.S-22.
[109] T. Fawcett, An introduction to ROC analysis, Pattern Recognit. Lett. 27 (8) (2006) 861–874, https://doi.org/10.1016/j.patrec.2005.10.010.
[110] Jr D.W. Hosmer, S. Lemeshow, R.X. Sturdivant, Applied Logistic Regression, John Wiley & Sons, New York, 2013, https://doi.org/10.1002/9781118548387.
[111] L. Menk, S. Terzi, M. Zebisch, E. Rome, D. Lückerath, K. Milde, S. Kienberger, Climate change impact chains: a review of applications, challenges, and opportunities for climate risk and vulnerability assessments, Weather Clim. Soc. 14 (2) (2022) 619–636.
[112] M. Zebisch, S. Terzi, M. Pittore, K. Renner, S. Schneiderbauer, Climate impact Chains—A conceptual modelling approach for climate risk assessment in the context of adaptation planning, in: C. Kondrup, et al. (Eds.), Climate Adaptation Modelling, Springer Climate. Springer, Cham, 2022, https://doi.org/10.1007/978-3-030-86211-4_25.
[113] S. Cocuccioni, F. Romagnoli, M. Pittore, I. Armas, D.T. Danila, G. Osaci, C. Albulescu, Ç. Göksu, S. Kundak, K.Y. Arslanlı, D. Kalkanlı, E. Özden Pak, B. Ergün Konukçu, T. Wenzel, P. Marr, E. de Zeeuw-van Dalfsen, L. Savelberg, P. Kalubowila, M. Hürlimann, M. Bockarjova, B. Witvliet, C. van Westen, F. Atun, The use of impact chains to describe complex cause-effect relationships within a systemic multi-sectoral and multi-hazard risk assessment, in: M.A. Erberik, A. Askan, M.K. Kockar (Eds.), Proceedings of the 7th International Conference on Earthquake Engineering and Seismology. ICEES 2023. Lecture Notes in Civil Engineering, vol 401, Springer, Cham, 2024, https://doi.org/10.1007/978-3-031-57357-6_38.